# Chapter 4

# Methanol Decomposition and Oxidation

Methanol decomposition and oxidation on noble metals are prototypical reactions in surface science because they serve as models for the interaction of alcohols or small organic molecules with catalysts (e.g. [79-83] and references therein). $CH_3OH$ dehydrogenation on Pd catalysts may provide a valuable source of hydrogen (e.g. for direct methanol fuel cells (DMFCs)) or of syngas, but only if the catalyst poison CO can be removed and if catalyst poisoning (deactivation) due to carbon deposition by methanolic C-O bond scission can be suppressed [13,14,84-86]. Furthermore, being the reverse reaction of methanol synthesis from CO and $H_2$ [87,88], $CH_3OH$ decomposition passes through the same intermediate steps and thus also provides insight into the synthesis reaction. Methanol oxidation can be regarded as test case to improve the total oxidation of volatile organic compounds (VOC´s), important in waste removal [89]. All the processes described would certainly benefit from an exact understanding of the reaction mechanism, which may eventually allow steering the reaction along the desired route.

In this chapter the interaction between methanol and Pd model catalysts will be investigated by XPS, PM-IRAS, STM, LEED and GC. The combined adsorption of methanol and oxygen will be also shown. Initially, methanol adsorption/desorption will be investigated under UHV conditions, as well as in a methanol pressure of $10^{-6}$ mbar on Pd(111) single crystal surface. Methanol decomposition on Pd(111) may proceed via dehydrogenation to CO and hydrogen or via C-O bond scission to carbonaceous species ($CH_x$), $CH_4$ and water. Under ultrahigh vacuum (UHV), Pd(111) is generally considered

inactive for $CH_x$ formation and the dehydrogenation pathway is favoured. In contrast, at higher pressure and temperature, significant amounts of carbon species were detected, suggesting a considerable activity of Pd(111) for methanolic C-O bond breaking. The morphology of the carbon deposit deriving from methanol decomposition was investigated by STM. The influence of surface defects on the scission of the methanolic C-O bond was addressed by creating defects by ion-bombardment of a Pd(111) surface. Methanol oxidation to $CO_2$, $H_2O$ and $CH_2O$ was followed by PM-IRAS, allowing a simultaneous detection of adsorbed and gas phase species, as well as by GC. Products of methanol decomposition were rapidly reacted away and only CO was observed during the reaction, which may be a spectator species. The oxidation state of Pd(111) was checked by post-reaction XPS, indicating that the reaction took place on metallic Pd, i.e. no evidence of Pd (surface) oxide was observed.

Methanol decomposition and oxidation were also investigated on alumina-supported Pd particles. Post-reaction XPS suggested that the Pd particles became partially oxidized during the methanol oxidation reaction.

In the last section the oxidation behaviour of different Pd model catalysts under UHV conditions will be discussed.

## 4.1 Methanol and Pd(111)

Previous studies of $CH_3OH$ decomposition on Pd(111) [74,80-83,90-105] reported activity for dehydrogenation while C-O bond scission activity was typically very small (or absent).

While there is general agreement that the dehydrogenation of methanol to CO and $H_2$ occurs *via* methoxy ($CH_3O$) as first intermediate, and is followed by stepwise hydrogen abstraction to $CH_2O$, CHO and CO [90-101], the mechanism and probability of C-O bond scission has raised some controversy.

The small methanolic C-O bond scission activity of Pd(111) was attributed to surface defects rather than to (111) terraces [79,83]. This agrees with the general opinion that defects are in many cases more active than terrace sites [106,107]. In contrast, *Chen et al.* [80] reported that methanolic C-O bond scission occurs *even on an atomically flat* Pd(111) surface but requires near monolayer methanol coverage. These authors suggested a

bimolecular mechanism producing $CH_3O$ (methoxy), $CH_3$ (methyl) and $H_2O$ by interaction of two neighboring $CH_3OH$ molecules. This model received further support by a recent molecular beam and DFT study [82]. When two $CH_3OH$ molecules come close together, the strong hydrogen bond between both molecules (mediated by one of the OH groups) may assist to break the methanolic C-O bond. These two models are quite different from each other, the first being defect-mediated and the second being related to inter-molecular interactions. For Pd nanoparticles on $Al_2O_3$ particle steps and edges were made responsible for C-O bond scission during methanol decomposition [105,108].

To gain further insight into these processes, the $CH_3OH$/Pd(111) system was revisited using a combination of X-ray photoelectron spectroscopy (XPS) and polarization-modulation infrared reflection absorption spectroscopy (PM-IRAS).

### 4.1.1 Methanol adsorption and desorption for multi- and (sub)-monolayer coverages on Pd(111)

In this section methanol dehydrogenation under adsorption/desorption (UHV) conditions on a smooth Pd(111) single crystal surface and on a "defect-rich" surface will be discussed. This reaction was investigated by "temperature-programmed-XPS (-PM-IRAS)", i.e. the Pd(111) surface was saturated at 100 K with 10 L (Langmuir; $10^{-6}$ Torr sec) and XPS (PM-IRAS) spectra were acquired at increasing temperature. For UHV experiments, the pressure indicated by the ionization gauge was corrected by the gauge sensitivity factor for $CH_3OH$ (1.9).

#### Methanol adsorption/desorption on smooth Pd(111) surface

Figure 4.1a shows C1s XPS spectra of 10 L $CH_3OH$ on Pd(111) acquired between 100 and 700 K (spectra shown only up to 400 K). The interpretation of the spectra was aided by previous XPS studies and by temperature-programmed desorption (TPD). TPD indicated desorption maxima at ~140 K for $CH_3OH$ multilayer desorption and at ~175 K for $CH_3OH$ monolayer desorption (not shown; see e.g.) [80].

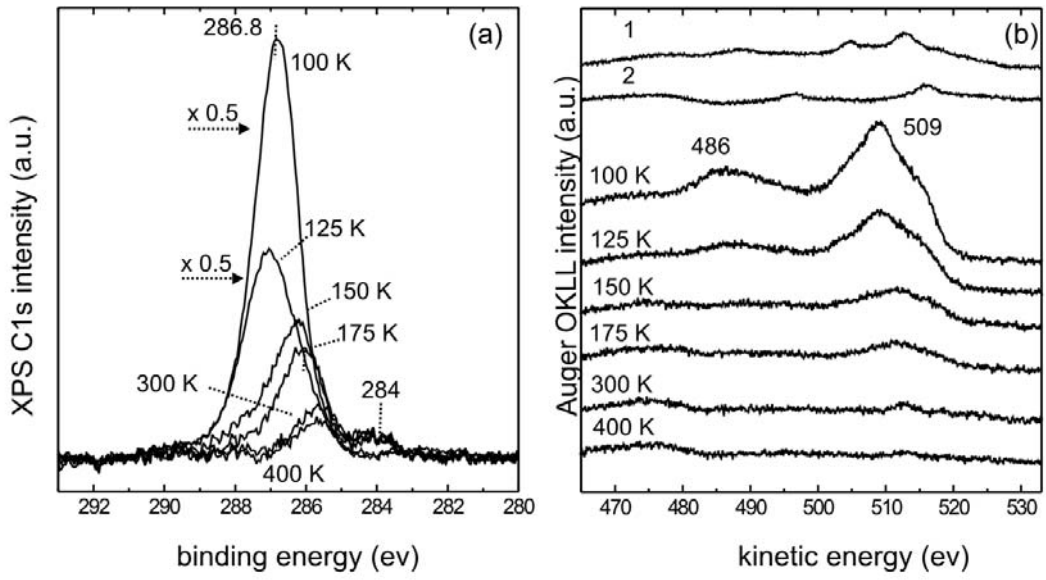


**Figure 4.1:** XPS spectra of methanol TPD on Pd(111). (a) XPS C1s core-level spectra and (b) corresponding oxygen KLL AES lines measured during $CH_3OH$ desorption between 100 and 400 K (exposure: 10 L $CH_3OH$ at 100 K). The reference spectra 1 and 2 in (b) were acquired in $5x10^{-8}$ mbar CO and $5x10^{-7}$ mbar $O_2$, respectively.

The analysis of the XPS data will start discussing the C1s signals around 286 eV, a binding energy value that may originate from $CH_3OH$, $CH_xO$ (x = 3-1) and CO. At 100 K, a $CH_3OH$ multilayer is present, producing a single C1s peak with a binding energy (BE) of 286.8 eV. Due to the thick $CH_3OH$ overlayer, almost no Pd3d signal was observed. At 125 K, the multilayer partially desorbed, as indicated by the intensity decrease and the small shift to 287.1 eV, and the appearance of a small Pd3d signal. Upon increasing the temperature to 150 K, the $CH_3OH$ multilayer desorbed and ~1 ML $CH_3OH$ remained (as indicated by a strong reduction of the C1s intensity, a shift to 286.2 eV and the clear appearance of Pd3d signals). Increasing the temperature to 175 K slightly reduced the C1s signal (coverage ca. 0.9 ML, assuming no changes in the C1s sensitivity factor) but the BE was shifted to 286.1 eV. Based on previous XPS and secondary ion mass spectrometry (SIMS) studies [80, 83] this indicates the onset of $CH_3O$ (methoxy) formation by O-H bond scission. At 200, 250 (not shown in Fig. 4.1a) and 300 K the C1s intensity further decreased (at 300 K the coverage is 0.15 ML) and the BE shifted to 286.1, 285.8 and 285.6 eV, respectively. Several processes occur simultaneously between 200 and 400 K: methanol

desorption, dehydrogenation of $CH_3O$ via $CH_xO$ to CO, and partial desorption of CO. The 285.6 eV peak at 300 K may in principle be due to $CH_xO$ and/or CO (~0.15 ML) but it is probably mostly CO. Previous HREELS studies [91,94,97] only detected CO at 300 K ($CH_3O_{ads}$-related features were only present after methanol adsorption at 200 – 250 K).

This indicates that an upper limit of about 20% of the $CH_3OH$ monolayer dehydrogenates to CO, in agreement with suggestions in the literature [80,82]. At 450 K, the C1s signal around 286 eV nearly vanished due to CO desorption.

O1s spectra may be an alternative way to discriminate between adsorbed CO and $CH_3O$. However, due to overlapping of O1s and Pd3p XPS signals, a clear interpretation of the data was not possible. The different surface orientation of CO (carbon downwards) and $CH_3O$ (oxygen downwards) may also influence the oxygen KLL Auger peaks. Therefore, the oxygen KLL Auger peaks were monitored during the stepwise annealing (Fig. 4.1b). Initially, when a methanol multilayer is present, the KLL peaks show a signature that is neither related to adsorbed CO [102] or oxygen on Pd(111), with two maxima at 509 and 486 eV (referring to the kinetic energy). The first is most likely the signature of the methanol monolayer and the second is due to the methanol multilayer structure, with the second and subsequent layers being weakly bonded (physisorbed). The change in the shape of the peaks from 125 to 150 K (with a shift in the main peak from 509 to 512 eV) and the disappearance of the peak at 486 eV may be due to the desorption of the multilayer. Other local chemical changes, e.g. loss of the hydrogen atom in the OH group, cannot be excluded though. During the further dehydrogenation of the methoxy group at 175 K and above, a small shift was again observed. This may indicate the rotation of the molecule but higher resolution and higher S/N XPS spectra are certainly required for confirmation.

In order to examine a possible C-O bond scission the C1s signals around 284 eV will now be discussed (Fig. 4.1a). A BE of ~284-284.5 eV is typical of carbon but hydrocarbon species ($CH_x$; x = 3-1) cannot be ruled out [109]. Figure 4.1a clearly indicates that no carbonaceous species were produced suggesting that C-O bond scission is absent or at least very limited ($\theta(CH_x)$ = 0.05 ML at 300 K) under the applied conditions and that $CH_3OH$ desorption dominates.

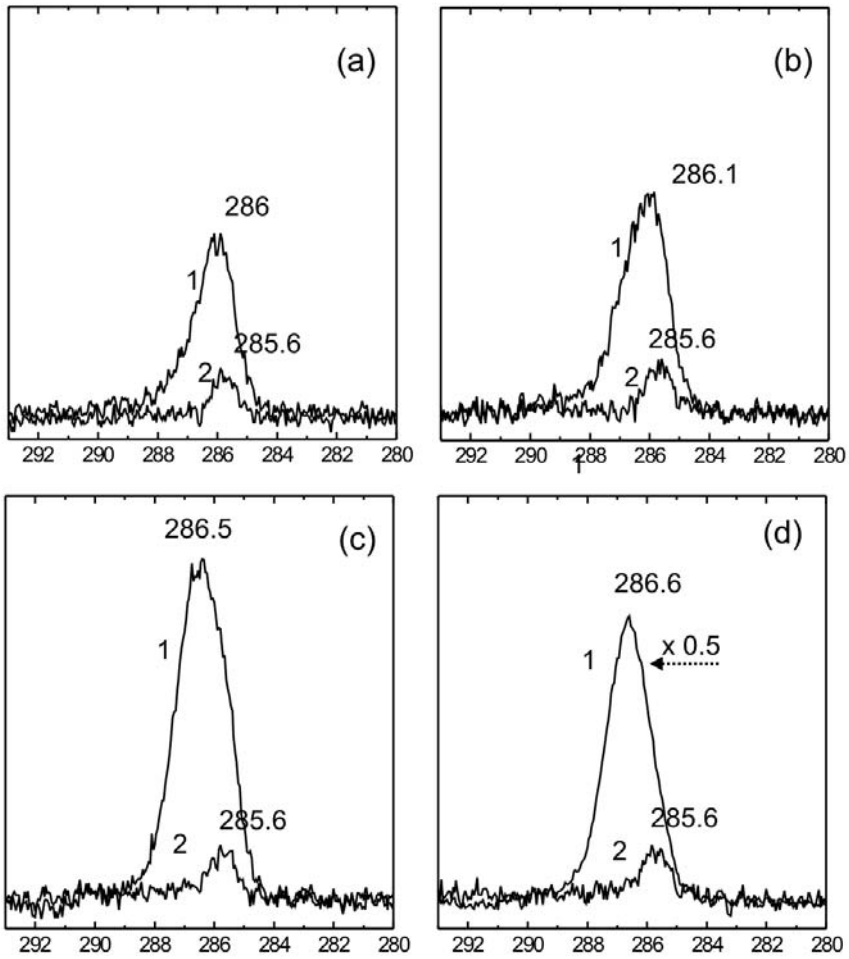


**Figure 4.2:** XPS C1s core-level spectra of $CH_3OH$ adsorbed on Pd(111) at 100 K (trace 1) and after direct annealing to 300 K (trace 2): (a) 0.7 L, (b) 1.0 L, (c) 2.3 L and (d) 3.7 L. After heating to 300 K, the CO coverage was quantified for the different methanol exposure: (a) $\theta_{CO}$ = 0.08 ML, (b) $\theta_{CO}$ = 0.09 ML, (c) $\theta_{CO}$ = 0.06 ML, (d) $\theta_{CO}$ = 0.07 ML.

Studies by the group of Winograd [80,102] suggested that a critical $CH_3OH$ coverage obtained by an exposure of 1 L at 100 K facilitates bimolecular interactions and thus promotes C-O bond cleavage. Higher (>2 L) or lower (<0.5 L) exposures did not produce carbonaceous species upon annealing. We have therefore also examined a range of different $CH_3OH$ exposures (~0.7-4 L). Figure 4.2 shows the C1s spectra for 0.7, 1.0, 2.3, and 3.7 L

$CH_3OH$ adsorbed at 100 K and subsequently heated to 300 K. However, under these conditions $CH_x$ formation was also not observed.

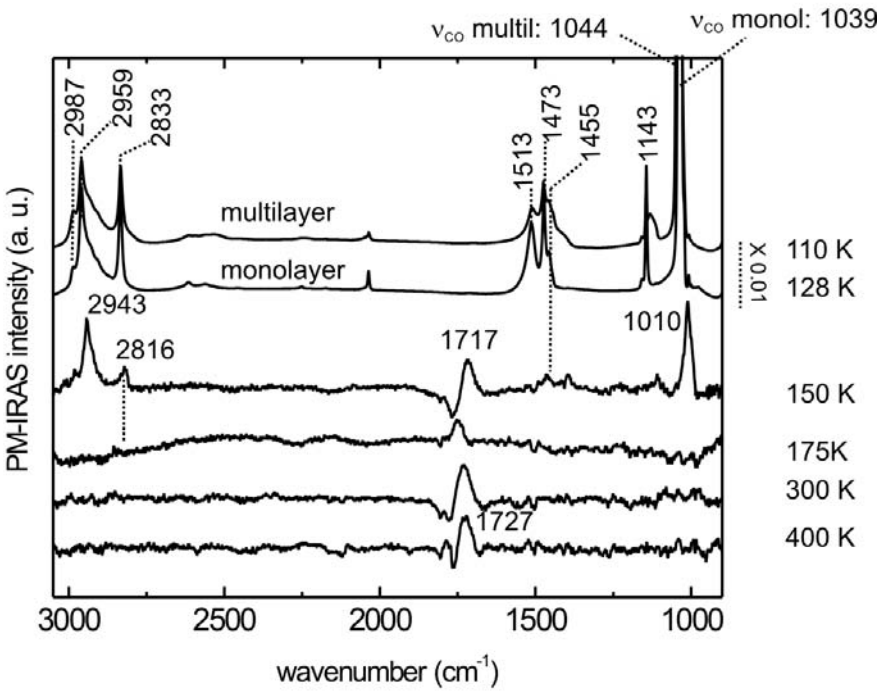


**Figure 4.3:** PM-IRAS spectra measured during $CH_3OH$ desorption between 110 and 400 K (exposure: 10 L $CH_3OH$ at 110 K).

Because XPS cannot fully differentiate between $CH_3OH$, $CH_xO$ and CO (with the resolution of a normal XPS setup), further experiments were carried out using infrared spectroscopy. Figure 4.3 shows a PM-IRAS spectrum of 10 L $CH_3OH$ on Pd(111) adsorbed at 110 K, with typical bands of the methyl group at 2959 $cm^{-1}$ ($\nu_{as}CH_3$) (with a shoulder at 2987 $cm^{-1}$), 2833 $cm^{-1}$ ($\nu_sCH_3$), 1513 $cm^{-1}$ ($\delta COH$), 1473 $cm^{-1}$ ($\delta_{as}CH_3$), 1455 $cm^{-1}$ ($\delta_sCH_3$), 1160 $cm^{-1}$ ($\rho_{as}CH_3$), 1143 $cm^{-1}$ ($\rho CH_3$), and of CO at 1045 $cm^{-1}$ ($\nu CO$). A very small CO signal at 2036 $cm^{-1}$ was observed, which rather originates from residual CO than from $CH_3OH$ decomposition [90,110]. This spectrum is characteristic of a methanol multilayer (the typical OH stretching mode at 3285 $cm^{-1}$ of molecular methanol could not be detected, since this region is affected by water condensed on the detector window). After annealing the surface to 128 K, a sharpening of the peaks is observed and $\nu CO$ is shifted to 1039 $cm^{-1}$. Weakly adsorbed methanol is desorbed and the spectrum at 128 K can be assigned to more

strongly chemisorbed methanol. By partial desorption of the monolayer at 150-175 K, the bands become weaker and shift in wavenumber. At 150 K bands are observed at 2943 $cm^{-1}$ ($\nu_{as}CH_3$), 2816 $cm^{-1}$ ($\nu_sCH_3$), 1107 $cm^{-1}$ ($\rho CH_3$) and 1010 $cm^{-1}$ ($\nu CO$). The main shift of the $\nu CO$ band to lower wavenumbers, when compared to the multilayer and monolayer (1045 and 1039 $cm^{-1}$, respectively), and the changes in the CH stretching region, suggest a dehydrogenation of the methanol at this temperature. The spectrum at 150 K can be therefore assigned to adsorbed methoxy. DFT calculations [111] have shown that methoxy intermediate prefers to be adsorbed on three-fold-hollow site on Pd(111).

A new band is also observed at 150 K around 1717 $cm^{-1}$, due probably to partial dehydrogenation of methoxy to CO.

By annealing the surface to higher temperatures, bands due to adsorbed methoxy are not any more detectable. The band attributed to CO slightly shifts with temperature.

The XPS and PM-IRAS data reported only small amounts of CO on the smooth Pd(111) surface, (ca. 0.15 ML CO, 0.05 ML $CH_x$), under the conditions reported, i.e. $CH_3OH$ mostly desorbs before it can react. The C-O cleavage activity of Pd(111) is rather negligible under UHV.

**Methanol adsorption/desorption on ion-bombarded Pd(111) surface**

As discussed in the introduction, the scission of the methanolic C-O bond was frequently attributed to surface defects. To address this issue defect-enriched Pd(111) was prepared by argon ion-bombardment. Systematic scanning tunneling microscopy (STM) studies of ion-bombarded transition metal surfaces have shown that high ion doses ($Ar^+$, $Ne^+$, $Xe^+$) produced surface defects such as vacancy pits [112,113]. These are the result of the nucleation and growth of vacancy islands inside other previously existing vacancy islands. The morphology of vacancy pits is quite characteristic, with many exposed atomic layers and with a high density of steps and kinks (for STM images see [112]).

By comparison with previous works [112,113] and by considering a sputter yield[1] for palladium of Y=1, we estimate that by the applied ion bombardment around 5-10 monolayers of Pd are removed and that approximately 50% of the surface atoms can be

[1] The sputtering of a surface is described by the "sputter yield" Y, which is defined as the mean number of sputtered target atoms per incident ion.

considered as defects. Morphological changes of the defective surfaces during the XPS experiments cannot be completely ruled out, especially when the surface is heated to 450 K or higher temperature. However, comparison with STM studies [112] rather suggests that at 450 K surface diffusion is not fast enough to fully anneal defects. *Kalff et al.* [112] have shown for Pt(111) that, even if the ion bombardment is carried out at 600 K, an extremely defective surface is produced for ion doses comparable to those applied in this work.

The surface defects generated in this way were subsequently characterized by PM-IRAS using CO as a probe molecule (see chapter 3, Figure 3.4). As already discussed, the defects created by ion-bombardment can be considered quite stable under the conditions applied here (450 K and below).

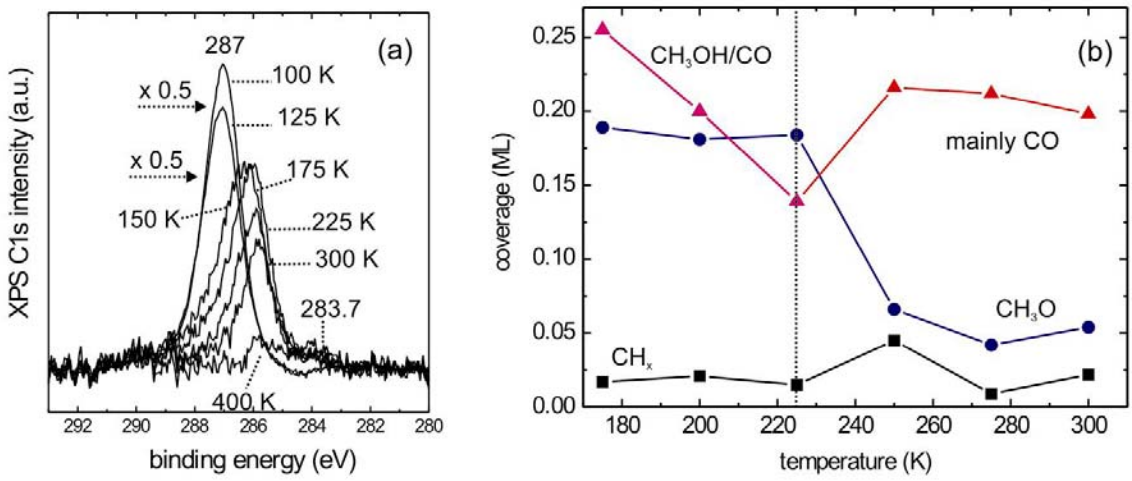


**Figure 4.4:** (a) XPS spectra of methanol TPD on an ion-bombarded Pd(111) surface in the C1s region. Initial exposure of 10 L $CH_3OH$ at 100 K, spectra acquired during $CH_3OH$ desorption between 100 and 400 K. (b) Coverage profile of the different species during methanol desorption between 175 and 300 K (initial methanol exposure: 10 L at 100 K).

In Figure 4.4a $CH_3OH$ adsorption/desorption on ion-bombarded Pd(111) is shown. Annealing to 300 K under UHV conditions again produced only small amounts of CO (peak at 285.6 eV) and almost no $CH_x$ formation was detected (small feature at ~283.7 eV). These results are very similar to $CH_3OH$ desorption/decomposition on well-annealed Pd(111) described in the previous section, indicating that C-O bond scission is not enhanced by surface defects under these conditions.

The interaction of methanol on the Pd(111) surface is quite different depending on the temperature and different products may be produced [114]. As already mentioned, several processes occur simultaneously between 200 and 400 K: methanol desorption, dehydrogenation of $CH_3O$ via $CH_xO$ to CO, and partial desorption of CO. Therefore, it is interesting to look more carefully at the C1s spectra previously discussed. The results of this analysis are reported in Figure 4.4b. Since the onset of $CH_3O$ (methoxy) formation by O-H bond breaking is around 175 K, a new fit of the C1s spectra during methanol desorption was performed from 175 K onwards, taking into account the simultaneous presence of methanol, methoxy, CO and $CH_x$ deposit on the surface. The black line with squares corresponds to the formation of $CH_x$ species, detected around 283.7 eV. Its coverage is always lower than 0.05 ML, indicating a small activity of Pd(111) in the methanolic C-O bond breaking. However, the presence of these $CH_x$ species already at 175 K, and its low binding energy could indicate that the small feature at ~283.7 eV is due to carbon impurity at the surface rather than to the formation of carbon deposit during methanol desorption. Anyway, the amount of carbonaceous species is negligible even at 300 K. The other two lines in Fig. 4.4b are correlated: the blue one with filled circles corresponds to methoxy (centered at 285.9 eV)[2] and the red-pink line with triangles corresponds to methanol and/or CO. The amount of methoxy is stable up to ~230 K, then it starts to dehydrogenate to CO (see the decreasing coverage). In parallel, the pink line before 230 K can be mainly attributed to methanol which is progressively desorbing with temperature. Above 230 K, the red line with triangles increases indicating the formation of CO from methoxy dehydrogenation.

The XPS chemical shift between methanol and CO and between methoxy and formaldehyde (another possible intermediate during dehydrogenation) can not be differentiated with the experimental setup used here. A more detailed investigation could be carried out using synchrotron radiation, which could give a higher resolution in order to differentiate among the different species and give a more specific conclusion.

### 4.1.2 Methanol decomposition at $10^{-6}$ mbar on Pd(111)

The results of the previous section indicate that the probability of dehydrogenation and C-O bond scission under adsorption/desorption conditions under UHV is apparently quite

[2] In the literature methoxy species on transition metal surfaces is reported at 285.8 eV.

small. $CH_3OH$ is mostly desorbed before the reaction onset temperature is reached. In order to generate a sufficient $CH_3OH$ surface coverage at elevated temperature (300, 450 and 550 K), experiments were also carried out in a background pressure of $10^{-6}$ mbar $CH_3OH$. The morphology of the carbon deposit formed at 300 and 450 K was also studied by STM.

**Methanol decomposition on smooth Pd(111) surface**

Figures 4.5a and 4.5b show XPS C1s spectra after exposing Pd(111) to $10^{-6}$ mbar $CH_3OH$ (total exposure time 510 min) at 300 and 450 K, respectively. At 300 K, two peaks were observed, at 285.6 eV due to $CH_xO$ and/or CO and at 284.2 eV due to carbon or carbonaceous species. Apparently, under these conditions dehydrogenation as well as C-O bond scission takes place. About 0.3 ML CO and about 0.5 ML $CH_x$ are observed at 300 K after 510 min. At 450 K, about 0.1 ML CO and about 0.8 ML $CH_x$ are found.

Fig. 4.5c shows the time dependent evolution of the different carbon species. The two peaks shown in Fig. 4.5a and 4.5b were deconvoluted to their respective components ($CH_x$ and $CH_xO$) and their concentration was quantified (using the (2x2)-CO structure at saturation coverage as reference.). The growth of the $CH_x$ species as a function of time can be readily observed, with the rate slowing down at the end, when saturation values are approached. It is clear that the $CH_x$ formation rate is faster and that the final hydrocarbon concentration is higher for the surface at 450 K. An important fact is that the CO formation (coverage) shows a close correlation with the $CH_x$ formation. At 300 K, after a fast initial CO growth, there is a decay and finally a constant - lower- CO coverage is obtained. For the sample at 450 K there is an initial slow growth and then again a constant CO concentration, which is always lower than that for the sample at 300 K. It seems that the lower the CO coverage, the faster is the $CH_x$ formation rate and the higher is the final $CH_x$ coverage. Higher temperatures apparently favor endothermic methanolic C-O bond scission but it seems that also the partial blocking of the surface with a high CO coverage at lower temperature can be a hindrance for this process. At 300 K the Pd(111) surface is at the beginning covered by almost 0.4 ML CO, and therefore the $CH_x$ amount is initially limited to only ~0.2 ML. The $CH_x$ amount increases progressively, but its production rate slows down due to a continuous blocking of Pd sites by CO and $CH_x$. At 450 K only 0.1 ML CO are present on the surface and the $CH_x$ production continues longer in time, finally producing ca. 0.8 ML carbonaceous species.

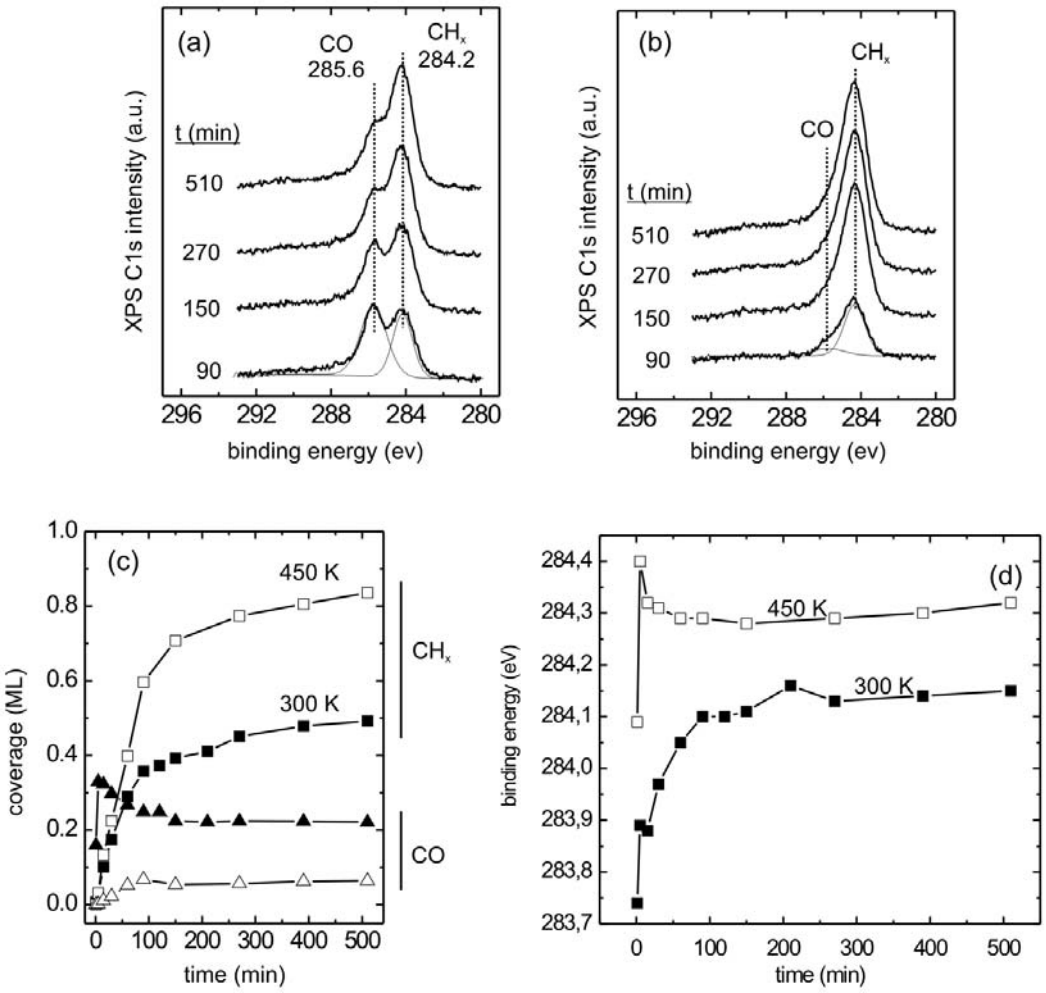


**Figure 4.5:** XPS C1s core-level spectra measured during $10^{-6}$ mbar $CH_3OH$ exposure on Pd(111) at 300 (a) and 450 K (b). The total exposure time was 510 minutes. (c) The relative amounts of CO and $CH_x$ species for both temperatures are also indicated. (d) The evolution of the binding energy of the carbonaceous species with time (or coverage) for both temperatures is reported.

The initial rate of $CH_x$ deposition is high both at 300 and 450 K. While the carbon coverage increases, there are less and less free sites on the surface, resulting in a decreasing rate in methanol decomposition (after 90 min at 300 K, and after 60 min at 450 K, see Fig. 4.5c). A similar kinetic effect was observed for methanol decomposition on Pd nanoparticles supported on alumina [78]. IRAS data suggested that the C-O bond breakage is fast only at defect sites (i.e. particle edges), which are then preferentially poisoned by $CH_x$ during the reaction, but not at the regular (111) facets. A contribution of C-O bond

scission on (111) facets could, however, not be excluded (since coupling effects make a quantitative analysis of IRAS spectra difficult). In addition, XPS studies on Pd nanoparticles (7000 ML methanol exposure at 440 K) revealed significant carbon amounts, which can not originate from carbon on particle-edges alone. In any case, the XPS results presented in this work at higher pressure ($10^{-6}$ mbar $CH_3OH$) indicate that the methanolic C-O bond scission takes place on the smooth Pd(111) surface. The role of surface defects will be further discussed in the following section related to methanol decomposition on ion-bombarded Pd(111) surface.

Fig. 4.5d shows the evolution of the binding energy of the carbonaceous species with time (or coverage; cf. Fig. 4.5a and Fig. 4.5b) for both temperatures. At 300 K, the BE shifts from initially 283.75 eV to 284.15 eV for the $CH_x$-saturated surface. According to a study by *Rodriguez et al.* [109], this may be interpreted as a transition from isolated carbon atoms to carbon clusters/islands. This suggests that isolated carbon atoms which result from C-O bond scission may act as nucleation centers for subsequently produced carbon atoms (diffusing over the surface), finally leading to carbon clusters. The carbon clustering shows a different behavior at 450 K. After a fast growth and decay in the initial moments of the exposure, the value of the binding energy for the carbonaceous species reaches a constant value around 284.3 eV, with a slow growing tendency. The higher temperature may have induced the formation of carbon deposit that may differ from the clusters formed by methanol exposure at 300 K.

In a recent study [115], a partial blocking of hollow sites by $CH_x$ (x = 0-3) fragments was observed by SFG after methanol exposure on smooth Pd(111). Based on previous theoretical studies [116,117], the authors suggested that the observed partial blocking of hollow sites was due to the presence of carbon atoms and/or CH species.

A combined XPS and STM study of $CH_3OH$ decomposition on Pd(111) was also performed. Further details about the morphology of the carbon deposits formed during extended $CH_3OH$ exposure on the Pd(111) perfect surface can be found in the corresponding section (see page 69).

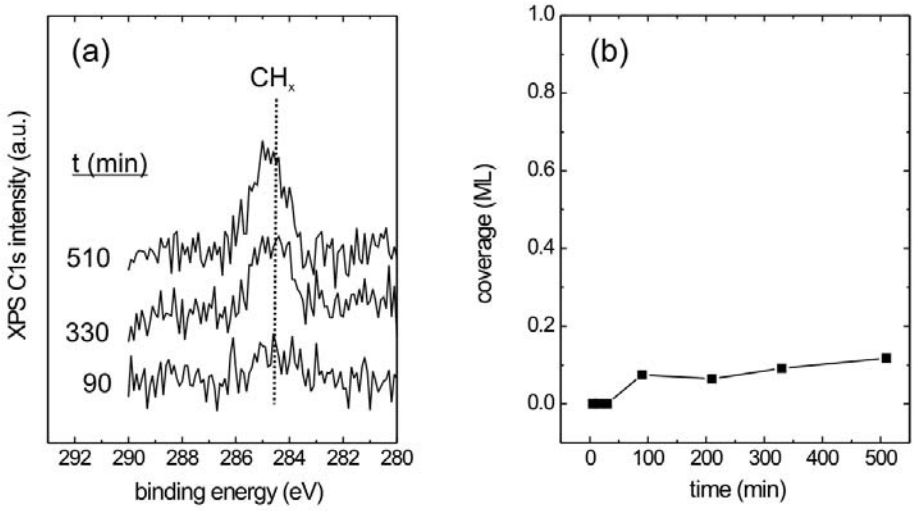


**Figure 4.6:** (a). XPS C1s core-level spectra measured during $10^{-6}$ mbar $CH_3OH$ exposure on Pd(111) at 550 K The total exposure time was 510 minutes. (b) The relative amounts of $CH_x$ species are also indicated.

From the XPS data shown in Fig. 4.5, it is evident that the methanolic C-O bond breaking is favored by higher pressure and temperature. The formation of $CH_x$ species is more important for the experiments performed at 450 K. The influence of temperature on the chemistry of methanol decomposition on the smooth Pd(111) surface was also investigated at 550 K. Figure 4.6 shows C1s XPS spectra after exposing Pd(111) to $10^{-6}$ mbar $CH_3OH$ (total exposure time 510 min) at 550 K. CO was not observed on the surface, because the experiment was carried out above the CO desorption temperature on Pd(111) ($T_{des}$ CO on Pd(111) = 450 K). After several hours of methanol exposure, the carbon amounts detected is only below 0.2 ML. This result is in disagreement with the enhancement on the breaking of methanolic C-O bond observed previously at higher temperature (Figure 4.5). Presumably at higher temperature (550 K) carbon migrated to subsurface region and then dissolved into the Pd bulk, being therefore not any more detectable by XPS. Migration of atomic carbon from a surface hollow site to an octahedral subsurface site is almost isoenergetic, as reported by a density functional study of *Yudanov et al* [118]. In the past [119], carbon dissolution in the Pd(111) single crystal was observed already at 470 K.

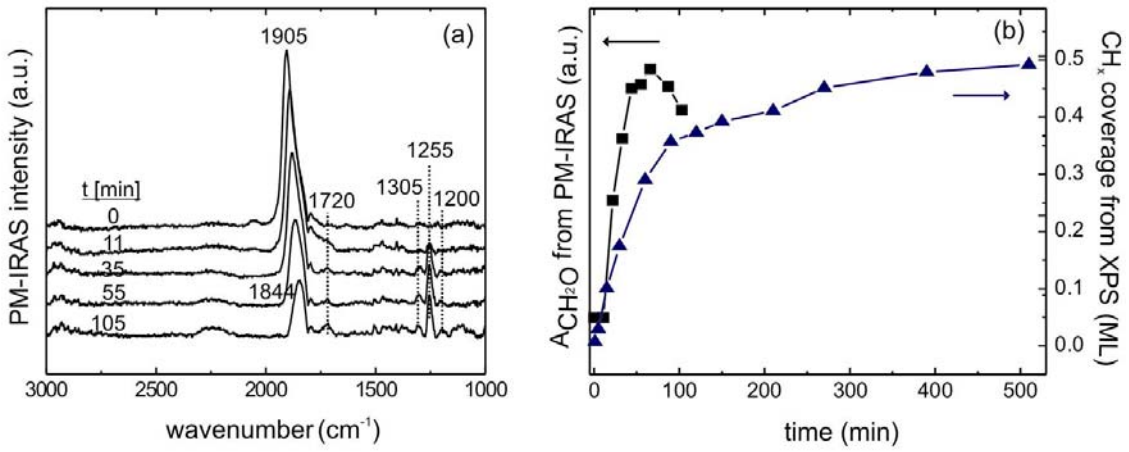


**Figure 4.7:** (a) PM-IRAS spectra measured during $CH_3OH$ decomposition on Pd(111) at ~$10^{-5}$ mbar and 300 K. In (b), the time dependent evolution of $CH_x$ (determined by XPS, see Figure 4.5) and of $CH_2O$ (determined by PM-IRAS) are compared.

Figure 4.7 compares PM-IRAS spectra and XPS data acquired during methanol exposure at 300 K. The PM-IRAS spectrum at time zero in Figure 4.7a revealed CO as only initial surface species with a coverage of ~0.4 ML (or lower), in agreement with XPS. Under UHV conditions methoxy, formaldehyde and formyl are typically not observed at this temperature, which might be due to the absence of $CH_x$ species. However, at ~$10^{-5}$ mbar PM-IRAS shows that formaldehyde and formyl surface species developed with time ($\rho CH_2$ of formaldehyde in two different adsorption geometries[3] at 1305 and 1255 $cm^{-1}$ [120]) and formyl CHO (CH bending or $\nu_{CO}$ at 1200 $cm^{-1}$ [121]). These species result from the dehydrogenation of methanol via methoxy, formaldehyde and formyl to CO [122]. Scheme 1 illustrates the decomposition (and oxidation, see section 4.1.3) of $CH_3OH$ on Pd(111), including those species which were experimentally detected.

[3] According to reference [120], formaldehyde is adsorbed in bridging and chelating geometry.

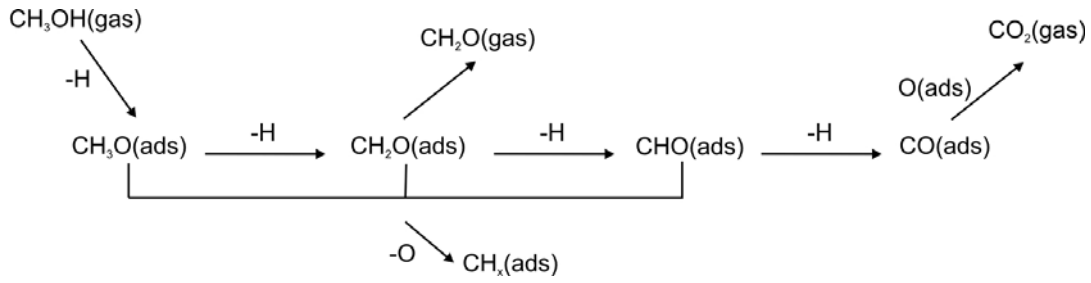


**Scheme 1:** Illustration on $CH_3OH$ decomposition and oxidation.

The growing peak around 1720 $cm^{-1}$ may be tentatively assigned to ν(C-O) of a formyl species or to ν(C-O) of formaldehyde [120]). The weak intensity of this peak suggests that $CH_2O$ is adsorbed with the C-O bond oriented nearly parallel to the surface.

One should note that under UHV conditions intermediate species of methanol decomposition were typically only observed at lower temperature. For instance, using HREELS *Davis and Barteau* [100] observed formaldehyde species around 170 K, finally leading to adsorbed CO and hydrogen atoms on Pd(111) at ~300 K. At 110 K CHO was observed by *Bhattacharya et al.* [94] during $CH_3OH$ decomposition on Pd(110). Using IRAS *Barros et al.* [120] observed formaldehyde on Ru(0001) at 190 K. However, the PM-IRAS spectra of Fig. 4.7a show that formaldehyde and formyl surface species developed with time during $10^{-5}$ mbar $CH_3OH$ exposure at 300 K, probably influenced by the presence of $CH_x$ species.

XPS can not differentiate between CO and $CH_2O$ but it indicated that the evolution of formaldehyde was paralleled by the evolution of $CH_x$ species (Figure 4.7b). As previously discussed, according to a recent study [115] $CH_x$ is most likely elemental carbon located in threefold hollow sites of Pd(111). However, "x" may in fact be 0 to 3 because C-O bond scission could basically occur within methoxy, formaldehyde and/or formyl (while no CO dissociation was observed [115]). Due to its adsorption geometry [123], formaldehyde seems to be the most likely precursor for C-O bond scission. A comparison between the time-dependent evolution of $CH_2O$[4] and $CH_x$ is displayed in Figure 4.7b which suggests that the formation of these species is in fact correlated. A possible explanation is that the carbon atoms prevent further dehydrogenation of formaldehyde to CO by poisoning the required (hollow) surface sites and/or by changing the electronic structure of neighboring Pd sites

[4] The relative amount was determined by integrating the PM-IRAS peaks at 1255 and 1305 $cm^{-1}$.

[124]. (*Barros et al.* [120] reported that CO stabilized formaldehyde on Ru(0001) but an influence of $CH_x$ could not be excluded because no XPS was performed). When the $CH_x$ coverage exceeded 0.4 ML the $CH_2O$ signal was reduced due to significant surface poisoning. The presence of $CH_x$ species hence has an influence on the different $CH_xO$ species formed during methanol dehydrogenation on Pd(111). An involvement of the $CH_x$ species for methanol oxidation will also be taken into account (section 4.1.3).

**Methanol decomposition on ion-bombarded Pd(111) surface**

Figures 4.8a and 4.8b show XPS C1s spectra during exposing $10^{-6}$ mbar $CH_3OH$ on an ion-bombarded Pd(111) single crystal surface (total exposure time 510 min) at 300 and 450 K, respectively. At 300 K (Fig. 4.8a), two peaks were again observed, at 285.6 eV due to CO and/or $CH_xO$ and at 284.2 eV due to carbon or carbonaceous species. Fig. 4.8c and 4.8d display the quantitative analysis of the evolution of the various species with time for both temperatures (at 300 and 450 K, respectively). Measurements on "smooth Pd(111)" are included (grey dotted lines) to allow a better comparison. We first consider the $CH_x$ formation. At 300 K (Fig. 4.8a and 4.8c) about 0.81 ML $CH_x$ were observed on ion-bombarded Pd(111) after 510 min. This is about *twice* as much as on smooth Pd(111). At first, this may suggest a higher activity of surface defects for C-O bond scission. On the other hand, since the defect concentration on ion-bombarded Pd(111) is at least 10-times higher than on smooth Pd(111), a twofold increase is not really a strong effect. A higher activity of surface defects can thus not be excluded, but it may not be a dramatic effect under the given conditions.

The higher amount of C-O bond breaking on the rough surface at 300 K may also be related to the reaction-diffusion behaviour of the adsorbed species. For instance, the probability that two methanol molecules meet and their methanolic bonds break (assuming a bimolecular mechanism, as proposed by Winograd [80,102], depends (among other factors) on the size of the domains (which constrains the accessible area of the diffusing molecules). For a rough surface, the size of the diffusion domains is strongly reduced [112,113], leading eventually to a higher probability that two molecules meet, which may lead to an increased amount of $CH_x$. This assumes, of course, that molecules can not cross via steps from one

terrace to the other due to the Ehrlich-Schwoebel barrier [125-127][5]. Another explanation for the observed increased activity in $CH_x$ formation on the rough Pd(111) surface could be a slight increase of surface area due to the presence of many steps, when compared to the surface area of the same sample without ion-bombardment ("smooth" surface). The increased surface area could allow more methanol molecules to adsorb and subsequently decompose, thus leading to a higher deposit of $CH_x$ species.

At 450 K, on ion-bombarded Pd(111) a final $CH_x$ concentration was obtained (0.85 ML). Under the same condition, a similar carbon amount was detected on the smooth Pd(111) (0.84 ML). A total annealing of the defects under the conditions applied can be excluded, as defects created by $Ar^+$-bombardment should be stable up to about 550 K [59]. The rate of $CH_x$ formation on the rough surface (Fig. 4.8d) is quite strange. In fact, when compared to the results obtained for the smooth surface (dotted line), the $CH_x$ formation rate is slower on the defect-rich surface. More experiments are probably needed in order to understand this particular behaviour at 450 K. The same measurements were repeated using different Pd(111) single crystals and the results are reproducible and compatible within the experimental error (~0.2%).

The CO formation on ion-bombarded Pd(111) (Fig. 4.8c and 4.8d) shows similar trends as on smooth Pd(111). At 300 K, the CO coverage decreases with time due to a continuous build-up of $CH_x$. At 450 K, despite the increasing amount of $CH_x$, the CO coverage slowly increases with time, but its value remains always below 0.1 ML.

The rate of C-O bond scission on both the smooth and ion-bombarded surfaces for both temperatures - (with exception for the measurement on the ion-bombarded surface at 450 K, as already discussed) – is fast at the beginning when the $CH_x$ concentration is still low and there are still many vacant sites on the surface. As the $CH_x$ coverage increases, a site-blocking mechanism decreases the rate of methanol decomposition.

[5] Actually the Ehrlich-Schwoebel barrier considers the probability that a step incorporates a diffusing adatom into itself. As the Ehrlich-Schwoebel barrier can affect crystal growth mode, several studies have been carried out for metal-on-metal systems. Nevertheless, this model has also often been assumed (and readapted) for gas atom or molecule diffusion on stepped metal surfaces [127].

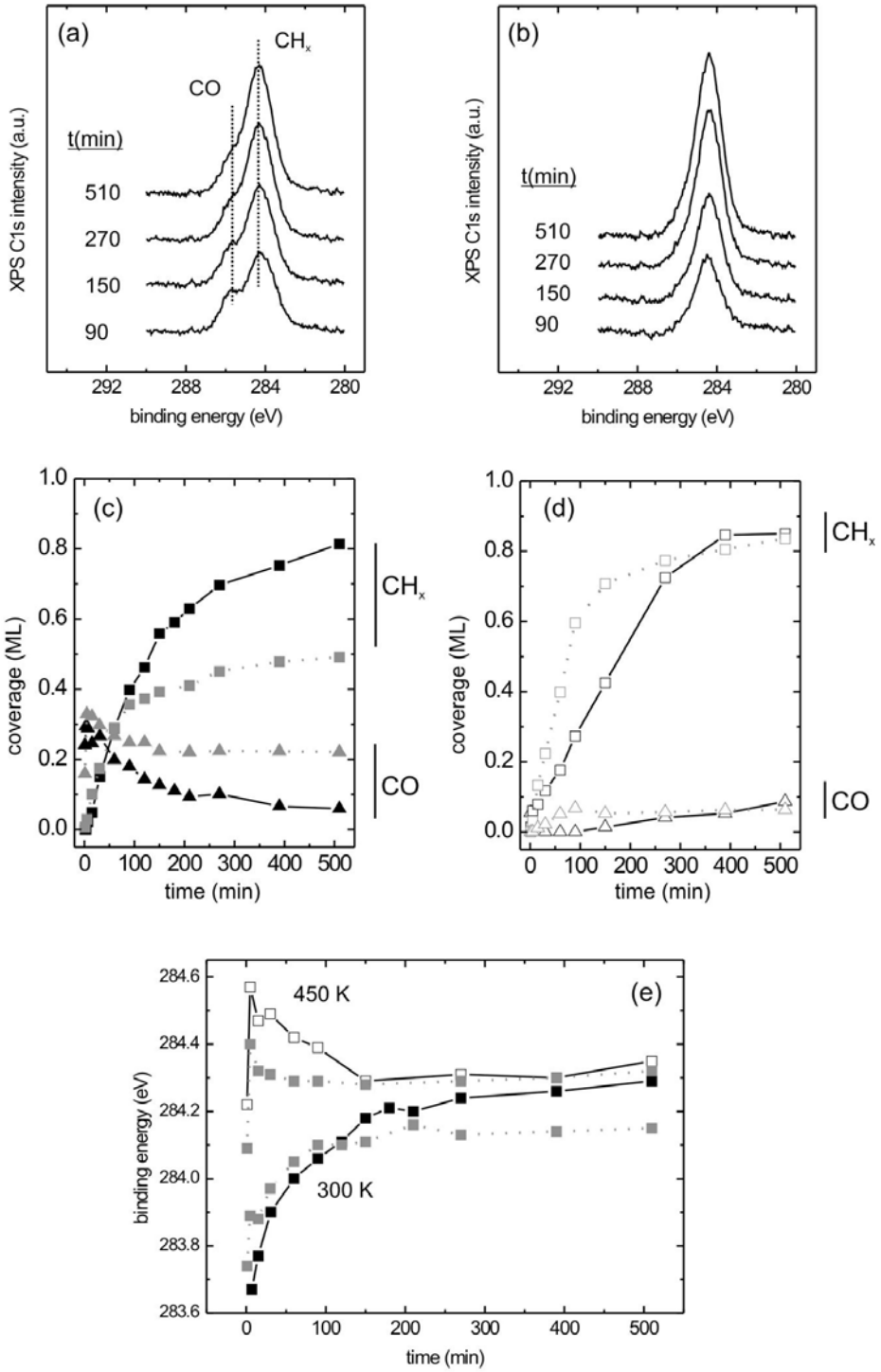


**Figure 4.8:** XPS C1s spectra measured during $10^{-6}$ mbar $CH_3OH$ exposure on ion-bombarded Pd(111) surface, at 300 K (a) and 450 K (b). (Total exposure time: 510 min). The relative amounts of CO and $CH_x$ species at 300 K (c) and 450 K (d) are also indicated. (e) The evolution of the binding energy of the carbonaceous species with time (or coverage) for both temperatures on the ion-bombarded surface is also reported (black line). The corresponding data for the smooth Pd(111) are also shown for comparison (grey dotted line).

Fig. 4.8d shows the evolution of the binding energy of the carbonaceous species with time. Within the experimental error, results on the ion-bombarded surface are very similar to those for the smooth Pd(111) surface.

**Methanol decomposition on smooth Pd(111) studied by LEED and STM**

Intermediate products of hydrocarbon decomposition reactions may have a significant role in catalysis as carbidic carbon appears to play an active role in catalytic processes [128,129]. It was shown previously in this work that carbonaceous species have an influence on the different $CH_xO$ species formed during methanol dehydrogenation on Pd(111) ([130] and Fig.4.7).

XPS data on methanol decomposition at $10^{-6}$ mbar pressure showed a considerable amount of carbon deposit both at 300 and 450 K. According to a recent study [109], it was suggested in this work that during $CH_3OH$ decomposition carbon clusters/islands grow on the Pd(111) surface rather than single carbon atoms. Unfortunately, the nucleation, growth and nature of these "carbon clusters" can not be deduced from XPS (or PM-IRAS). Therefore, methanol decomposition was studied combining results from angular-resolved XPS with the structural and morphological information obtained by LEED and Scanning Tunnelling Microscopy (STM). The Pd(111) single crystal used to perform STM measurements was the same employed for the methanol reactions previously discussed.

Figure 4.9 reports STM images of the Pd(111) surface after the standard cleaning procedure described in Section 2.5. As can be observed in Fig. 4.9a, the sample is characterized by large (111) terraces, separated by straight step edges. The height of the Pd steps is ~2.7 Å (close to the Pd-Pd distance of 2.75 Å), suggesting monoatomic steps. In Fig. 4.9b the Pd 1x1 mesh can be resolved.

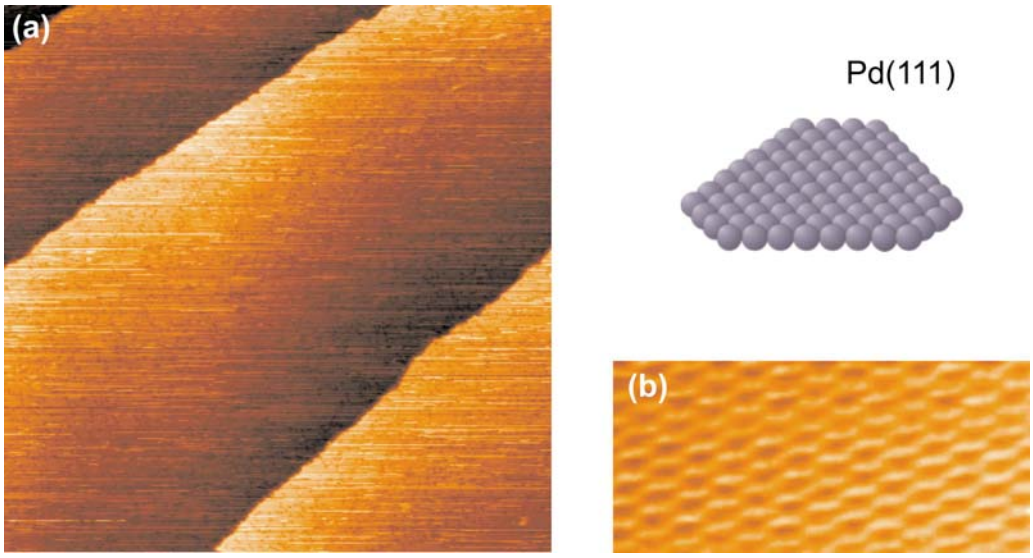


**Figure 4.9:** STM images of nominally clean Pd(111) surface: (a) 100x100 nm image (tunnelling conditions: $I_t$ = 1.0 nA, $V_t$ = 0.05 V); (b) 1.4x3.0 nm image, resolving the Pd 1x1 mesh ($I_t$ = 1.0 nA, $V_t$ = -0.05 V). From top to bottom the image is slightly compressed due to a drift of the piezoelectric elements. A schematic representation of the hexagonal structure of the single crystal is also reported.

In order to avoid contamination of the STM tips, the sample was then transferred under UHV to a separated treatment chamber (base pressure of ~$1x10^{-10}$ mbar) where methanol exposure (about $10^{-6}$ mbar) was performed at 300 K at increasing exposure time. After each exposure, the sample was analyzed by means of XPS, STM and LEED. Methanol was also dosed on Pd(111) at 450 K in order to check the influence of temperature on the breaking of the methanolic C-O bond and the subsequent formation of carbonaceous species.

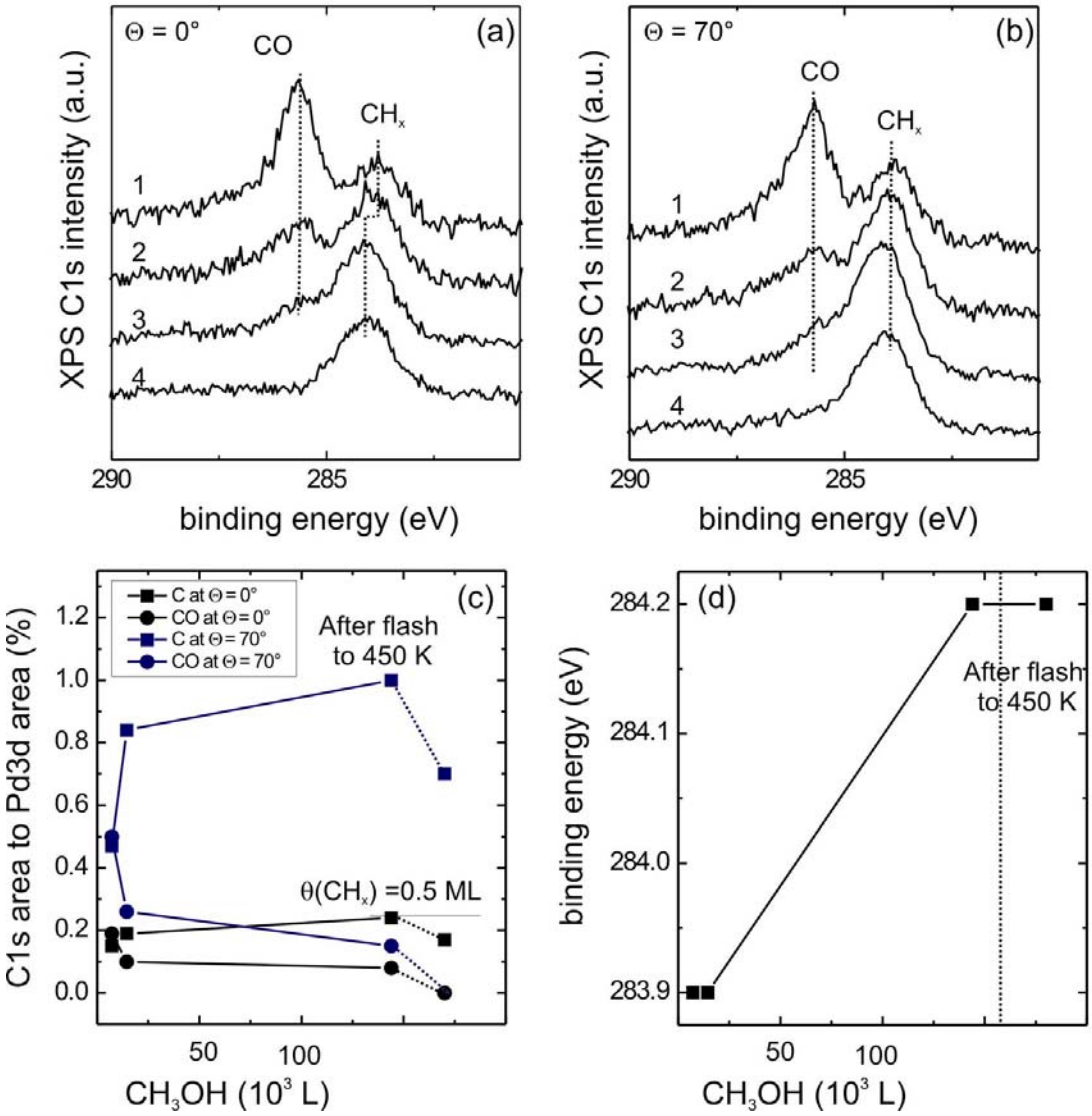


**Figure 4.10:** Angular resolved XPS C1s core-level spectra measured during $CH_3OH$ exposure on Pd(111) at 300 K at Θ = 0° (a) and at Θ = 70° (b): 7200L (trace 1); 36000L (trace 2); 360000L (trace 3); after flash to 450 K (trace 4). The C1s intensities at Θ = 0° and at Θ = 70° were normalized at 275 eV. (c) The relative amounts of CO and $CH_x$ species for both angles of acquisition are also indicated. (d) The evolution of the binding energy of the carbonaceous species with $CH_3OH$ exposure is reported.

Figure 4.10a and 4.10b show XPS C1s core-level spectra acquired at different electron emission angle Θ - (Θ = 0° and Θ = 70°, respectively) - after exposing methanol on Pd(111) at 300 K for increasing exposure time (traces 1-3). As already observed in Fig. 4.5, two peaks are detected at ~285.6 eV and ~284 eV, which are attributed to CO and $CH_x$ species, respectively. After the final $CH_3OH$ exposure (traces 3), the sample was flashed to 450 K to

desorb CO (traces 4). The XPS spectra were fitted and deconvoluted to obtain the areas of the CO and $CH_x$ components. The ratio between these areas and the Pd3d area is plotted in Fig. 4.10c. Using the (2x2)-3CO saturation structure of CO on Pd(111) (coverage 0.75 ML) as reference (assuming identical sensitivity factors for CO, C and $CH_x$), the amount of CO and $CH_x$ for the measurements at $\Theta = 0°$ can be directly compared with the results previously reported in Fig. 4.5c for $CH_3OH$ decomposition at 300 K followed in the "PM-IRAS chamber". The two sets of data are in good agreement, showing an upper $CH_x$ coverage of ~0.5 ML (see arrow in Fig. 4.10c). The values obtained for the measurements performed at $\Theta = 70°$ are higher than those performed at a zero degree electron emission angle. Variation of the electron emission angle $\Theta$ allows altering the degree of surface sensitivity. At higher values of $\Theta$, higher surface sensitivity is reached. Therefore, as the $CH_x$ area to Pd3d area ratio is higher for measurements at $\Theta = 70°$, it is possible to conclude that the carbonaceous species formed during methanol decomposition reside mainly on the surface. The binding energy of this carbonaceous species shifts from ~284.1 eV to 284.4 eV as the coverage increases. This behaviour was already observed (Fig. 4.5d) and it can be interpreted as a transition from carbon "chains" to carbon clusters [109]. After flashing the sample to 450 K (traces 4), CO is completely desorbed while the amount of $CH_x$ slightly decreases due to partial migration to subsurface regions of Pd(111). The BE of this carbonaceous species is anyway not affected by the flash to 450 K, indicating that the nature of the "carbon clusters" is not significantly changed.

In the following, STM and LEED images acquired after the different methanol exposures will be discussed.

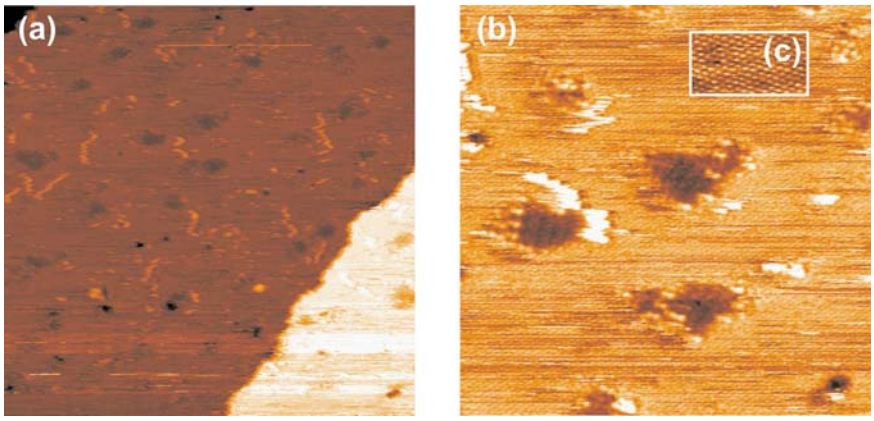


**Figure 4.11:** STM images after 7200 L $CH_3OH$ ($10^{-6}$ mbar for 2 hrs) at 300 K on Pd(111). (a) 50x50 nm; (b) 20x20 nm; (c) 2.3x4.3 nm ($I_t$ = 1.0 nA, $V_t$ = -0.1 V).

Figure 4.11 shows STM images of Pd(111) after 7200 L methanol exposure ($10^{-6}$ mbar for 2hrs) at 300 K. The step edges appear now rough and irregular, while terraces are more or less evenly decorated by aggregates of different shape. The Pd step height is similar to that of clean Pd(111) (~2.7 Å) and the Pd 1x1 structure can still be resolved, as reported in Fig. 4.11c.

XPS data indicated that both CO and $CH_x$ species are formed on the surface during methanol decomposition (Fig. 4.10, traces 1). CO molecules diffuse rapidly on the surface already at 190 K [44]; therefore it is impossible to image them with a room temperature STM. The bigger agglomerates are better resolved in the 20 nm x 20 nm image (Fig. 4.11b). They have an average dimension of (2.5x5) nm and their observed protrusion (close to a hexagonal arrangement) is about 7.3 Å. It is reasonable to associate these agglomerates with (monolayer thick) carbonaceous small particles resulting from methanol decomposition. In particular, these small particles are randomly distributed on the Pd(111) surface and are not concentrated only at step edges. *Land et al.* [131] followed ethylene dehydrogenation on Pt(111) by STM and observed as well the formation of carbon containing particles dispersed randomly across the sample. The same authors concluded that Pt steps did not show any preferential reactivity for ethylene dehydrogenation. An enhancement of methanolic C-O bond scission on step edges can not be totally excluded though, as the STM measurements were performed after 2 hours methanol exposure. Nevertheless, it is evident that also (111) terraces are involved during methanol decomposition and subsequent formation of carbon deposit.

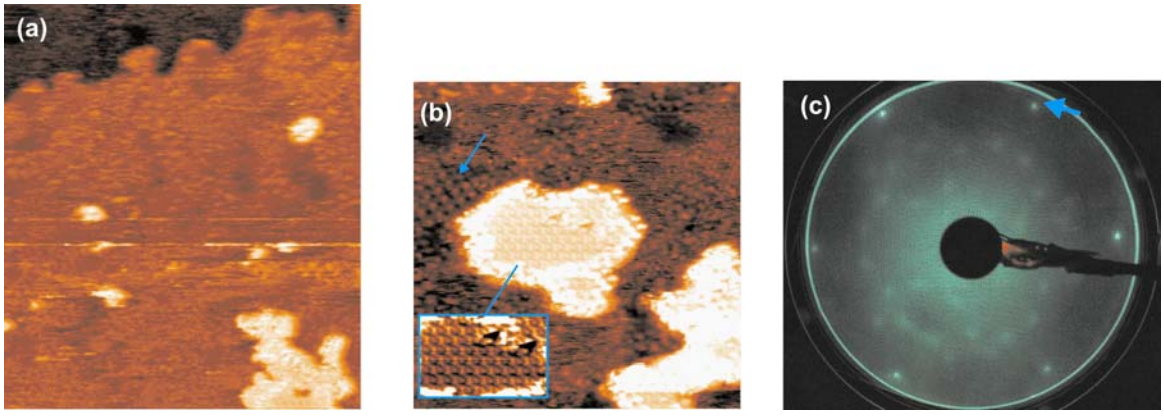


**Figure 4.12:** (a) 32x14 nm and (b) 20x20 nm STM images of Pd(111) after 36000L $CH_3OH$ exposure ($5x10^{-6}$ mbar for 2 hrs) at 300 K ($I_t$ = 1.0 nA, $V_t$ = -0.1 V). (c) Corresponding LEED pattern at 300 K ($E_{el}$ = 60 V) is reported. The arrow in the LEED image points on a Pd(111) reflex.

Methanol exposure was repeated under stronger conditions. Figure 4.12 shows STM and LEED images of Pd(111) after 36000 L methanol exposure ($5x10^{-6}$ mbar for 2 hrs) at 300 K. According to XPS (Fig. 4.10, traces 2), the amount of $CH_x$ species is increased, leaving less space for CO to adsorb. The step edges appear even more irregular than what was observed after the first methanol exposure, but the Pd step height has not changed (~2.7 Å). The carbonaceous agglomerates are visible all over the Pd surface. Some of these agglomerates have probably coalesced, forming bigger islands of irregular shape (average dimensions: (6x10) nm). In fact, the density of the carbon-covered area has increased with respect to what was observed after the first methanol exposure (7200 L) reported in Fig. 4.11. The average height of these islands is ~2.3-2.4 Å, corresponding to one C layer. During ethylene decomposition on Pt(111) the formation of similar particles was followed by STM [131]. The height distribution of carbonaceous particles formed at higher temperature gave an average value of 2.3 Å. The authors thus concluded that this value corresponded to the formation of monolayer high carbon particles. As previously suggested in this work, the $CH_x$ species formed during methanol decomposition on Pd(111) should be mostly elemental carbon [115-117].

Two big carbon islands are visible in the (20x20) nm image of Fig. 4.12b. An ordered superstructure pattern is visible on the top of the islands (see also inset in Fig. 4.12b). This superstructure has a hexagonal arrangement with unit cell of ~7 Å. On the top left side of the central island in Fig. 4.12b a different ordered structure is observed (see arrow), whose periodicity is again ~7 Å. This ordered structure is observed randomly on the whole Pd surface. In a previous work [132], after benzene exposure at high temperature on Pt(111), non-graphitic carbon islands were observed on the substrate by STM. The observed carbon layer presented a hexagonal pattern with a periodicity of 12.1 Å. *Ueta et al.* [133] observed the formation of highly oriented monolayer graphite by the collision of supersonic methane molecules with sufficient kinetic energy (670 meV) on a Pt(111) surface. The corresponding STM images showed moiré superstructures with different periods of ~9 Å and of ~7.4 Å, rotated respectively by 15° and by 19.1° with respect to the Pt(111) substrate.

The corresponding LEED pattern (Fig. 4.12c) shows still the hexagonal arrangement of the Pd atoms from the substrate (see arrow), while new diffuse ring diffraction spots are now visible (a detailed analysis of the LEED data will be given during the discussion of Figure 4.14). Former studies of hydrocarbon dehydrogenation on Pt(111) have reported similar LEED images, which were associated with the characteristic ring diffraction pattern of graphite [133,134].

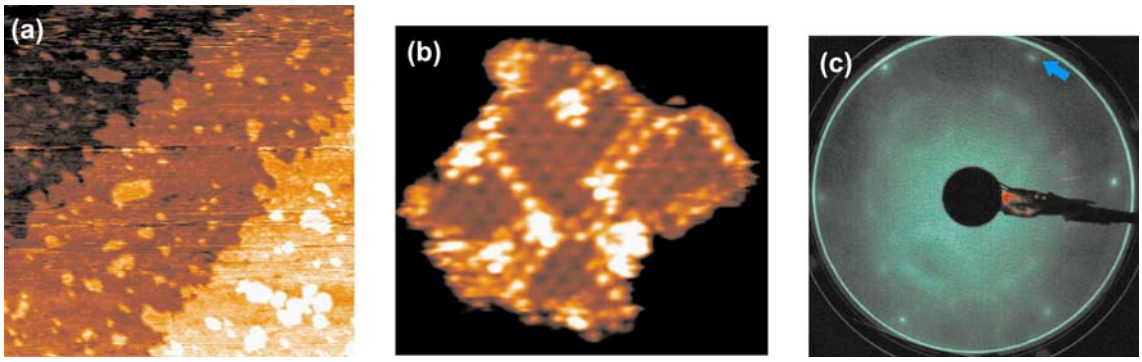


**Figure 4.13:** (a) 100x100 nm and (b) 12x10.6 nm STM images of Pd(111) after 360000L $CH_3OH$ exposure ($2x10^{-5}$ mbar for 2 hrs) at 300 K ($I_t$ = 0.5 nA, $V_t$ = -0.1 V). (c) The corresponding LEED pattern at 300 K ($E_{el}$ = 60 V) is reported.

Figure 4.13 shows STM and LEED images of Pd(111) after 360000 L $CH_3OH$ exposure ($2x10^{-5}$ mbar for 2 hrs) at 300 K. The carbon formation is increased, while CO has less and less space on the surface to adsorb (see XPS data of Fig. 4.10, traces 3). Surprisingly, even though the step edges are severely "eaten" the Pd step height is kept constant (~2.7 Å). The roughness of the step-edge lines suggests a rearrangement of the Pd atoms. A similar phenomenon was reported previously in the literature by *Fujita et al.* [132] after long exposure of benzene at high temperature on Pt(111), and by *Land et al.* [131] after ethylene exposure at elevated temperature on Pt(111). The authors suggested two different growth behaviours of the observed carbon overlayers. In the first case [132], the authors suggested that the Pt atoms were trapped at the step edges covered with a graphene sheet and that, as a consequence, the graphene sheet grew on the lower steps at the same rate as that on the upper steps. In the second work [131], the step roughening was explained by a hindering effect of the carbon adsorbed at the step toward the 2D evaporation of Pt atoms from the Pt step to the terrace. Pt atoms from the clean area of the step could rapidly move close to step sites pinned by adsorbed carbon. A more precise model to explain the roughness of Pd steps (due to the formation of methanol-derived carbon islands) can not be suggested in this work, but it is evident that the rearrangement of Pd atoms is related to the formation of these carbon islands.

By increasing methanol exposure (thus increasing the formation of $CH_x$ species), larger islands grow together with the formation of smaller structures and the density of the carbon islands increases. Interestingly, carbon islands are still randomly distributed all over the

surface. A (12x10.6) nm STM image of a carbon island is reported in Fig. 4.13b. The island height is still ~2.3 Å and the hexagonal arrangement has still a unit cell of ~7 Å Domains of different superstructure orientation can be observed, separated by antiphase domain boundaries (brighter lines).

The corresponding LEED pattern (Fig. 4.13c) still shows the spots of the Pd substrate (see arrow), together with diffuse ring-aligned spots due to the carbon overlayer, but the background is very diffuse.

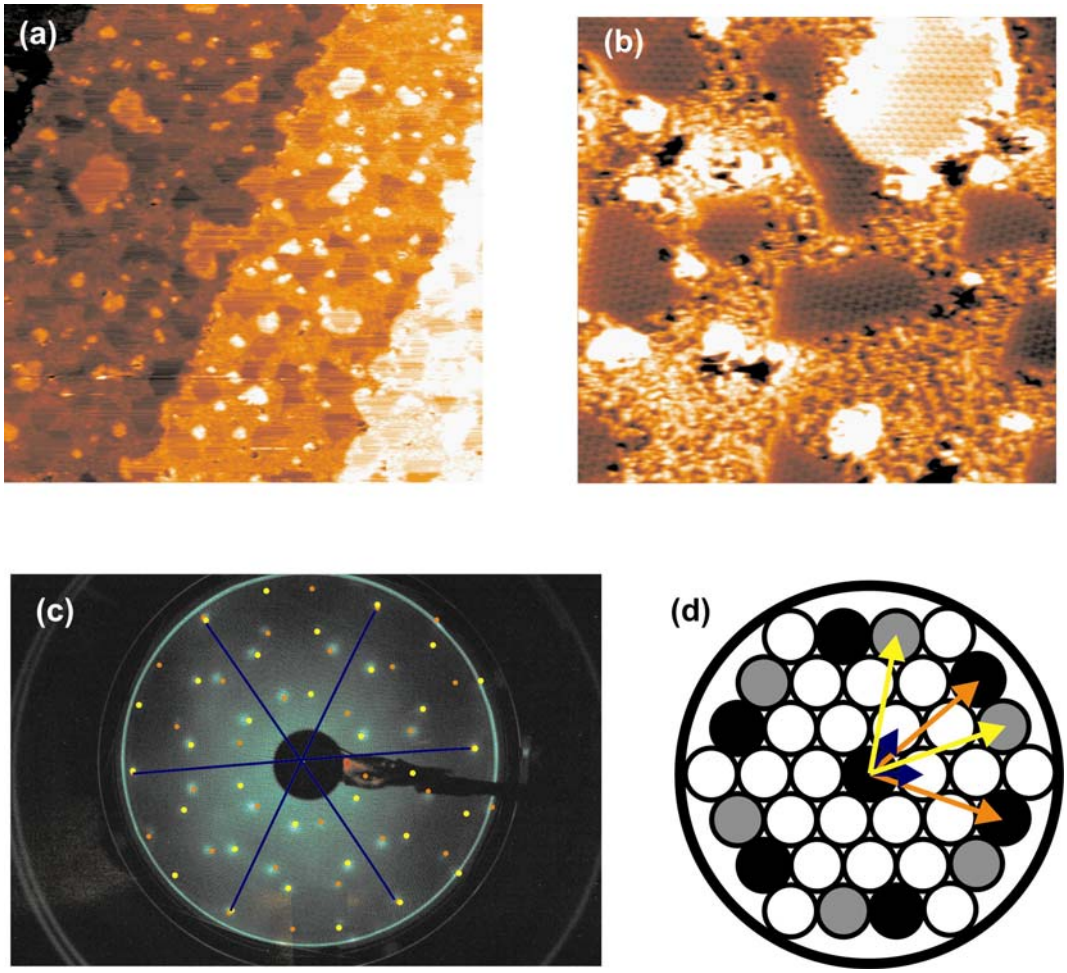


**Figure 4.14:** (a) 100x100 nm ($I_t$ = 1.0 nA, $V_t$ = -0.1 V) and (b) 30x29.2 nm ($I_t$ = 0.5 nA, $V_t$ = -0.2 V) STM images of Pd(111) after 360000L $CH_3OH$ exposure at 300 K and subsequent flash to 450 K. (c) The corresponding LEED pattern at 300 K ($E_{el}$ = 60 V) is reported. The blue lines in the LEED image show the diffraction spots related to Pd, while the yellow and orange circles indicate the diffraction spots from two different carbon overlayers. (d) A schematic representation of the hexagonal arrangement of the Pd atoms (open circles) is also shown. The two carbon overlayers are represented by grey and black circles. The different lattice vectors are also reported.

After the last methanol exposure (360000 L), the surface was flashed to 450 K in order to desorb CO. As can be observed by the corresponding XPS analysis (Fig. 4.10, traces 4), no CO is detected after this treatment, while the amount of carbon species is slightly reduced, due probably to partial migration of $CH_x$ species into subsurface regions. Anyway, the nature of the carbon structures should not be strongly affected, as the corresponding BE does not shift (Fig. 4.10d) and the average size of the islands, as seen from the (100x100) nm images, is not drastically changed. Due to the short anneal to 450 K a better ordering of the carbon islands can be observed.

The whole surface is decorated by carbon islands, which dimension is comparable with the carbon islands observed before flashing to 450 K (average height: ~2.3 Å). Also islands of smaller dimension, about (4x5) nm, exhibit an ordered superstructure after the flash to 450 K. As can be observed in Fig. 4.14b, the carbon islands are of different irregular shape and are differently oriented on the Pd(111) substrate, but the unit cell is still ~7 Å. The surrounding surface areas appear disordered in the STM pictures.

In the corresponding LEED pattern (Fig. 4.14c) the ring-aligned diffraction spots are now clearly visible. The LEED pattern analysis reported a $(\sqrt{7}x\sqrt{7})R19.1°$ overlayer structure for the carbon overlayer. Two carbon overlayers can be recognized (see orange and yellow points in the LEED pattern) which are rotated by 21.77° with respect to each other and with lattice vector of 7.28 Å. These two carbon overlayers are simply domains rotated in different orientation, as can be seen in the scheme shown in Fig. 4.14d. The LEED pattern is consistent with the hexagonal structure with unit cell of ~7 Å observed by STM.

In a previous study of benzene exposure on Pt(111) [132], a similar LEED pattern was observed and was consistent with a $(\sqrt{19} \times \sqrt{19})R23.4°$ structure of the carbon layer.

Methanol was also exposed on Pd(111) at 450 K ($5x10^{-6}$ mbar for 2 hrs; 36000 L). As already observed in this work (Fig. 4.5b and c), higher temperatures apparently favour methanolic C-O bond scission leading to a higher carbon formation. At $\Theta$=0° the ratio between the area of $CH_x$ and the Pd3d area is equal to ~0.6%, while at $\Theta$=70° is ~2.3%. For the measurements at $\Theta$=0° the given ratio corresponds to ~1 ML (using the (2x2)-CO structure at $\Theta$=0° as reference). When comparing this values with those obtained for methanol exposure at 300 K (Fig. 4.10c), it is evident that during exposure at 450 K more carbon deposit have been formed.

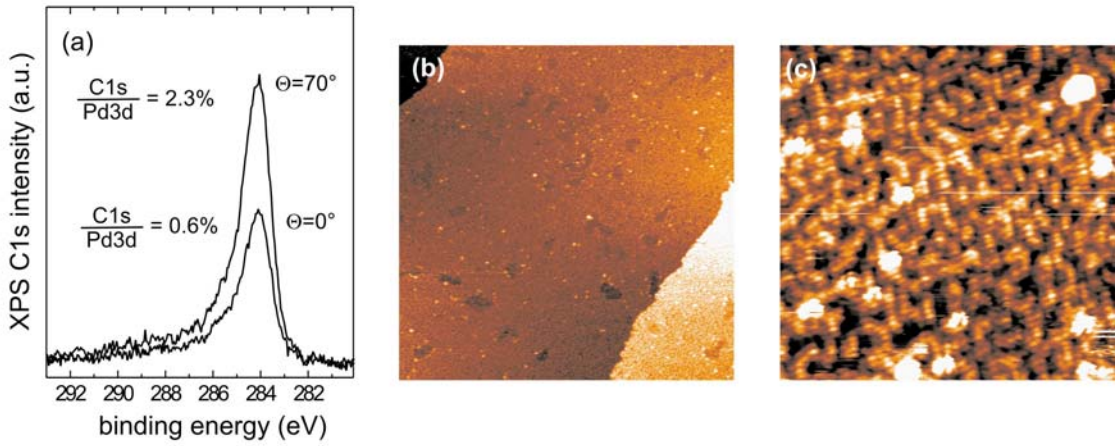


**Figure 4.15:** (a) XPS in the C1s region, (b) (100x100) nm STM image ($I_t$ = 1.0 nA, $V_t$ = -0.1 V), and (c) (15x15) nm STM image ($I_t$ = 1.0 nA, $V_t$ = 0.1 V) after 36000L methanol exposure ($5x10^{-6}$ mbar for 2 hrs) on Pd(111) at 450 K.

After $CH_3OH$ exposure at 450 K, the whole surface appears covered by a meandering structure. The Pd step height is still ~2.7 Å and almost straight and the step edges appear still regular as for clean Pd(111). From the (15x15) nm STM image (Fig. 4.15c), this meandering structure appears to be formed by round particles, but it was not possible to better resolve it. Pd diffraction spots can not be observed in the corresponding LEED image (not shown). The carbon overlayer can not as well be observed by LEED due to its disordered arrangement.

The different carbon structures formed by methanol exposure at 300 K and at 450 K on Pd(111) may be related to a "kinetic effect". As already observed from XPS measurements (Figure 4.5), the formation of $CH_x$ is faster and the final $CH_x$ coverage is higher at 450 K. As a consequence, carbon atoms have probably less time to diffuse on the surface and to cluster together to form bigger and ordered islands (as observed instead for methanol exposure at 300 K). Moreover, as Pd atoms are very fast decorated by a bigger amount of carbon, they are completely hindered and can not migrate and thus the Pd step edges appear almost regular in the corresponding STM images.

Summarising, the UHV studies of methanol decomposition indicated that desorption and dehydrogenation dominated and that Pd(111), both the smooth and the ion-bombarded single crystal, was rather inactive for methanolic C-O bond breaking. The XPS and PM-IRAS experiments indicated that methanol mostly desorbed upon annealing before it could react (see Fig 4.1, 4.3, 4.4, 4.7). In contrast, already at methanol pressure of $10^{-6}$ mbar, significant amount of carbonaceous species could be detected by XPS (see Fig. 4.5 and 4.8), and their presence should be taken into account for a catalytic reaction. The morphology and structure of the carbonaceous deposit was investigated using STM and LEED. Exposure of Pd(111) to methanol at 300 K led to the formation of monolayer thick (2.3 Å) carbon islands of irregular shape. The hexagonal arrangement of the carbon overlayer has a unit cell of ~7 Å and LEED analysis reported a (√7x√7)R19.1° overlayer structure. By increasing methanol exposure at 300 K on Pd(111), the density of these carbon islands increases, as well as their dimension. As already suggested, isolated carbon atoms from methanolic C-O bond scission may act as nucleation centres for subsequently produced carbon atoms, leading to the formation of carbon clusters, which dimension increases with increasing methanol exposure.

The formation rate of carbon is faster when methanol is exposed at 450 K. XPS measurements reported as well a higher amount of carbon deposit (close to 1 ML). A meandering disordered carbon structure is formed all over the Pd(111) surface after methanol exposure at 450 K.

In the following section the chemical stability of the carbon deposit (formed during methanol decomposition) towards oxygen will be investigated.

### 4.1.3 Methanol oxidation on Pd(111)

Methanol oxidation on Pd(111) was studied at elevated (mbar) pressure employing a combination of in situ PM-IRAS, on-line gas chromatography (GC), and pre- and post-reaction XPS [130]. The influence of carbonaceous overlayers that are present during the reaction will be discussed. It will be shown that the presence of carbon species may not only act as poison, but also be involved in driving the selectivity for methanol oxidation. The

oxidation state of the catalyst surface after the mbar reaction was checked by post-reaction XPS.

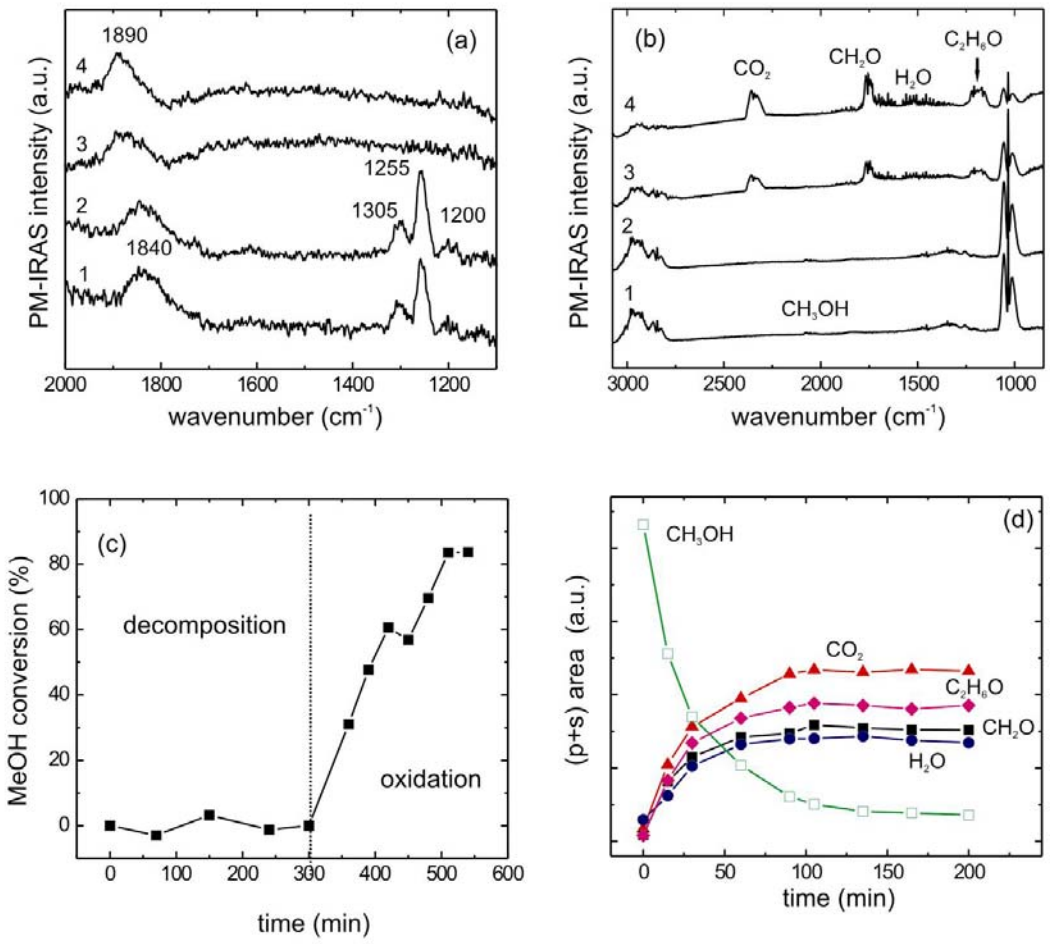


**Figure 4.16:** (a) Surface (p-s) and (b) gas-phase (p+s) PM-IRAS spectra measured during $CH_3OH$ oxidation at 300-400 K (5 mbar $CH_3OH$ added at 300 K (trace 1) prior to 5 mbar $O_2$ (trace 2)). Spectra 3 and 4 were acquired during the oxidation reaction at 400 K, after 15 and 60 min, respectively. Methanol conversion and formation of $CO_2$, $H_2O$ and $CH_2O$, (and $C_2H_6O$), as measured by gas chromatography and PM-IRAS (p+s) spectra, are displayed in (c) and (d), respectively.

Figure 4.16 shows PM-IRAS surface (p-s) and gas phase (p+s) spectra acquired during methanol exposure and oxidation at mbar pressure. The gas phase composition, as determined by GC[6] and PM-IRAS, is shown in Fig. 4.16c and Fig. 4.16d, respectively. After exposing 5 mbar $CH_3OH$ to Pd(111) at 300 K, PM-IRAS identified adsorbed CO ($\nu$CO at ~1840 $cm^{-1}$, typical of ~0.3 ML coverage) as well as peaks of formaldehyde ($\rho CH_2$

[6] For the GC experiment, 15 mbar $CH_3OH$, 15 mbar $O_2$ and 1050 mbar Helium as carrier gas were used.

of formaldehyde in two different adsorption geometries at 1305 and 1255 $cm^{-1}$ [120] and of formyl CHO (bending or νCO at 1200 $cm^{-1}$) (Fig. 4.16a, spectrum 1). These species result from the dehydrogenation of methanol via methoxy, formaldehyde and formyl to CO [121]. Apart from these species, $CH_x$ carbonaceous overlayers in excess of 1 ML were observed by in situ [115] and post-reaction XPS (Fig. 4.18c). Hence, in the absence of oxygen the surface is poisoned by CO, $CH_2O$, (CHO) and $CH_x$. As a result, no activity for methanol decomposition was detected by GC analysis (Fig. 4.16c) and also corresponding PM-IRAS gas phase spectra only detected the reactant $CH_3OH$ (Fig. 4.16b). As already mentioned, intermediate species of methanol decomposition were typically only observed at lower temperature under UHV [94,100,120].

Upon oxygen addition, all surface species remained almost stable up to 350 K. The onset of catalytic activity was observed at 400 K, with $CH_2O$, $CO_2$ and $H_2O$ identified as gas phase products by GC and PM-IRAS (p+s) spectra (Fig. 4.16c and 4.16d). The $CH_3OH$ conversion after 3h at 400 K was ~84%, yielding a turnover frequency of 7/site sec (initial turnover frequency of 15/site sec after 90 min of reaction), and with a product distribution of ca. 10% $CH_2O$ and 25% $CO_2$. Both GC and PM-IRAS also detected ethanol. On the surface, PM-IRAS detected only CO while formaldehyde and formyl had disappeared. Apparently, at 400 K $CH_2O$ and CHO were reacted away, either by dehydrogenation to CO and/or by desorption. The amount of $CH_x$ under reaction conditions, as deduced from XPS, was 0.4 ML (Fig. 4.18c, trace 2) (The peak at 284.3 eV is due to $CH_x$, the peak at 285.6 eV originates from CO. The two "bumps" in trace 1 (clean surface) are "Pd-satellites" due to the non-monochromatic X-ray source and do not originate from adsorbed species). The reduced amount of $CH_2O$ and $CH_x$ under reaction conditions generated more free surface sites and led to a higher CO surface coverage, indicated by the shift of the CO peak to ~1890 $cm^{-1}$ (typical of ~0.4 ML CO) (Fig. 4.16a, traces 3 and 4).

From these observations, it can be concluded that methanol oxidation proceeds via dehydrogenation to $CH_2O$, which either desorbs or is further dehydrogenated to CO, which is subsequently oxidized to $CO_2$ (scheme 1). During the various dehydrogenation steps, reaction of hydrogen and oxygen produces, of course, water. Apparently, the surface concentration of $CH_2O$ (and CHO) is below detection limit under reactive conditions.

An involvement of the $CH_x$ species in steering the selectivity for methanol oxidation is also suggested in this work. It is plausible, in fact, that $CH_x$ may favour $CH_2O$ formation by hindering its dehydrogenation to CO. One observation supporting this suggestion is that, at

reaction temperatures of 500 K or higher, when the $CH_x$ concentration is much smaller (Figure 4.18c, trace 3), only $CO_2$ and water were observed as products in PM-IRAS (p+s) spectra (not shown). Furthermore, the correlation between the formation of $CH_2O$ and the presence on $CH_x$ deposit during methanol decomposition on Pd(111) was already shown (Fig. 4.7b).

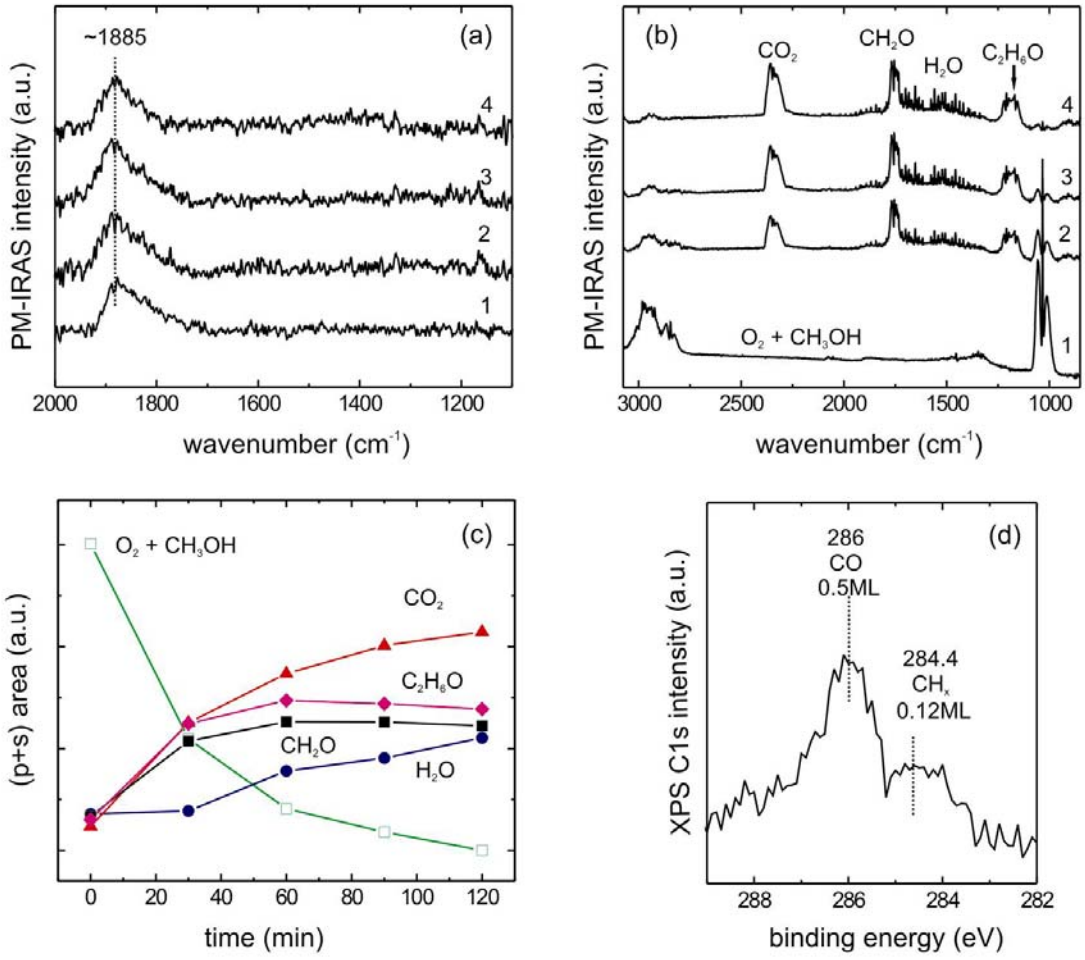


**Figure 4.17:** (a) Surface (p-s) and (b) gas-phase (p+s) PM-IRAS spectra measured during $CH_3OH$ oxidation at 300-400 K (5 mbar $O_2$ added at 300 K prior to 5 mbar $O_2$ (trace 1)). Spectra 2, 3 and 4 were acquired during the oxidation reaction at 400 K, after 30, 60 and 90 min, respectively. Methanol conversion and formation of $CO_2$, $H_2O$ and $CH_2O$ (and $C_2H_6O$), as measured by PM-IRAS (p+s), are displayed in (c). (d) XPS spectrum in the C1s region after 90000 L $O_2$ added prior to 90000 L $CH_3OH$ at 300 K.

Figure 4.17 shows PM-IRAS surface (p-s) and gas phase (p+s) spectra acquired during methanol exposure and oxidation at mbar pressure, when 5 mbar $O_2$ were added at 300 K on Pd(111) prior to 5 mbar $CH_3OH$. The gas phase composition determined by PM-IRAS (Fig.

4.17c) shows the same activity as for the inverse gas dosage (methanol added prior to $O_2$ (Fig. 4.16)). The onset of catalytic activity was observed at 350-400 K, with $CH_2O$, $CO_2$ and $H_2O$ identified as gas phase products by PM-IRAS (p+s) spectra (Fig. 4.17b). Again ethanol was detected as gas phase product by PM-IRAS. Adsorbed CO (νCO at ~1885 $cm^{-1}$, typical of ~0.4 ML coverage) was the only species identified on the surface at 300 K and during the reaction at 400 K. The oxygen atoms already adsorbed on the surface at 300 K block surface sites where products of methanol decomposition reaction ($CH_2O$, CHO) can reside. A temperature of 350-400 K or higher is needed in order to start the reaction. The XPS spectrum of Fig. 4.17d shows the oxygen inhibiting effect on the methanolic C-O bond breaking at 300 K. The Pd(111) surface was exposed to 90000 L $O_2$ at 300 K and subsequently saturated with 90000 L $CH_3OH$ at the same temperature. The XPS spectrum in the C1s region shows two peaks at 286 and 284.4 eV, corresponding to CO and $CH_x$ species, respectively. The amount of carbon deposit was calculated to be only $\theta(CH_x)$ = 0.12 ML. This value is much lower than the amount of carbon deposit observed for methanol decomposition at 300 K on clean Pd(111) ($\theta(CH_x)$ = ~0.5 ML, Fig. 4.5), due to the presence of oxygen atoms on the surface.

Partial and total methanol oxidation can go through different complex intermediate reactions. A possible reaction pathway for the production of $CH_2O$, $CO_2$ and water in the gas phase was already described previously in this work (see also scheme 1). The PM-IRAS (p+s) spectra analysis for both “dosing conditions” (Fig. 4.16d and 4.17c) showed also the development of ethanol as gas phase product. As no traces of ethanol were observed in the gas phase spectra of pure methanol, a possible contamination of the reactant can be excluded. The formation of ethanol during methanol oxidation at mbar pressure may possibly originate from the interaction of methyl groups (or $CH_x$ fragments) derived from C-O bond breaking with adsorbed oxygen atoms and/or CO molecules. Another possible pathway could go through the interaction of formate (HCOO) species with other fragments derived from methanol decomposition. Anyway, this second pathway seems less probable because formate was not observed by PM-IRAS (neither as adsorbed species nor formic acid as gas phase product). In previous works, *Endo et al* [135-137] observed by IRAS a peak around 1330 $cm^{-1}$ during deep oxidation of methanol on Pt(111). The authors assigned that peak to the O-C-O symmetric stretching mode of formate, adsorbed vertical to the surface in a bridging configuration. The molecularly adsorbed oxygen was considered to be responsible for the oxidation of methanol to formate. However, the peak observed in this

work at 1255 $cm^{-1}$ during methanol decomposition and oxidation (Fig. 4.7 and 4.16, respectively) is rather assigned to (chelating) formaldehyde, which is also observed in the (p+s) PM-IRAS gas phase spectra. Furthermore, the post-reaction XPS spectra (Fig. 4.18c, traces 2 and 3) did not show any formate signal at ~288.5 eV [109,138,139].

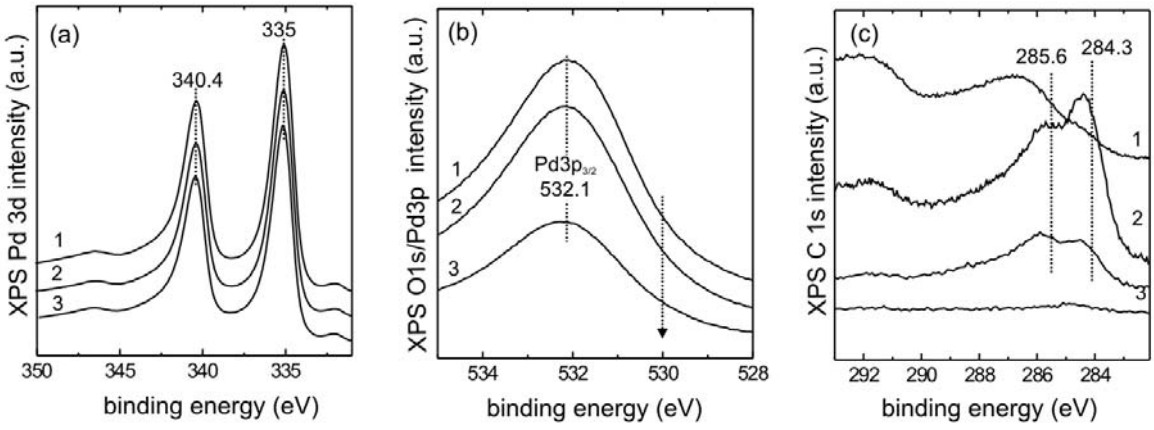


**Figure 4.18:** Pre- and post-reaction XPS spectra in the Pd3d (a), O1s/Pd3p (b), and C1s (c) region: Pd(111) as prepared (trace 1); after the mbar reaction of Figure 4.16 at 400 K (trace 2); after mbar reaction at 500 K (trace 3).

An interesting question regards the state of the Pd(111) surface during the oxidation reaction at millibar pressure at 400 K (or higher). Surface oxides of Pd ($Pd_5O_4$ overlayer) and of other metals have recently raised much attention and may contribute to a reaction by supplying oxygen or by constituting the active phase [140,141]. Former studies of Pd(111) oxidation reported chemisorbed oxygen in the p(2x2) structure (0.25 ML) at 529.2 eV [142] while oxygen features from the two-dimensional oxide, $Pd_5O_4$, were observed at ~529.5 eV [143]. Figure 4.18 shows the pre- and post-reaction XPS for methanol oxidation at mbar pressure at 400 K and 500 K (trace 2 and trace 3, respectively). Post-reaction XPS in the O1s/Pd3p region did not indicate any surface oxidation (Fig. 4.18b, traces 2 and 3). The Pd3d region also only detected metallic Pd (Fig. 4.18a, traces 2 and 3), but may not be sensitive enough, because ~5-10 Pd layers are probed using a standard Mg anode and a possible oxidation of the first layer could be undetected. More surface sensitive spectra can be obtained using low photon energy, which results in a lower kinetic energy of the photoelectrons and therefore only the very first surface layers are detected. Considering the metallic component of the clean Pd(111), the $Pd3d_{5/2}$ peak is usually reported at 334.9 eV.

The slight shift to 335.0 eV (Fig. 4.18a, trace 1) observed in this work reflects the increase of the bulk contribution due to the high photon energy used ($MgK\alpha$ = 1253.6 eV), which increases the information depth (the binding energies of the Pd bulk and surface components are reported at 334.9 and at 334.6 eV, respectively [142]). Further information about the state of the Pd(111) surface can be obtained by PM-IRAS spectra, which showed that the CO species observed during the oxidation reaction were typical of adsorption on *metallic* Pd. Therefore, it can be concluded that the oxidation of the Pd(111) surface, if present at all, must be minor under the reaction conditions for methanol oxidation at 400 and 500 K.

Further studies on Pd(111) oxidation at $10^{-5}$ mbar oxygen will be presented in the last section of this chapter. A comparison between Pd(111) single crystal, Pd(111) thin film on NiAl(110) and Pd nanoparticles will be discussed as well.

## 4.2 Methanol and $Pd/Al_2O_3/NiAl(110)$

As shown in the previous section, although methanol decomposition and oxidation are considered model reactions, they consist of several steps and different competing reaction pathways even on the unsupported Pd(111) single crystal surface.

In this section we focus on the interaction of methanol with a supported Pd model catalyst, i.e. $Pd/Al_2O_3/NiAl(110)$. Methanol decomposition and oxidation on alumina supported Pd particles have been extensively studied under UHV conditions [78,105,144,145]. Recently, also high pressure measurements have been performed by means of SFG [37].

The aim of this work was to add complementary information to the SFG study of methanol interaction with supported Pd catalyst under relevant conditions, and to overcome some limitations of SFG spectroscopy (i.e. the limited vibrational range). Therefore, PM-IRAS experiments were performed under high $CH_3OH$ pressure. Unfortunately, the PM-IRAS intensity of these spectra was quite small. Probably, C-O bond breaking on Pd particles under high pressure is much faster and the resulting amount of $CH_x$ deposit on the surface is too high, so that no good signal is detectable by PM-IRAS at millibar pressure.

### 4.2.1 Methanol adsorption and desorption for multi- and (sub)-monolayer coverages on $Pd/Al_2O_3/NiAl(110)$

In the introduction to this section, a brief discussion about methanol adsorption on alumina film will be presented. Former TPD, IRAS and SFG studies [137,144,145 and references therein] reported molecular adsorption of methanol on the pristine $Al_2O_3$ film on NiAl(110). In the thesis of *Morkel* [37], TPD experiments reported a small desorption peak at 215 K for low $CH_3OH$ dosage on the alumina film, while for increasing exposure (up to 0.35 L) a desorption peak at 175 K was observed. The desorption peak at 175 K was attributed to methanol monolayer desorption from regular $Al_2O_3$-sites, while the peak at 215 K was attributed to desorption from defect sites. When the initial $CH_3OH$ dosage was increased (>0.5 L), a new peak at 140 K was observed, due to multilayer desorption of methanol. *Schauermann et al.* [144,145] reported two distinct coverage-dependent desorption states at 190 K and 170 K for the submonolayer absorption of methanol on the same $Al_2O_3$/NiAl(110)-system. The authors attributed these peaks to methanol desorption from defects sites (peak at 190 K) and from regular oxides sites (peak at 170 K).

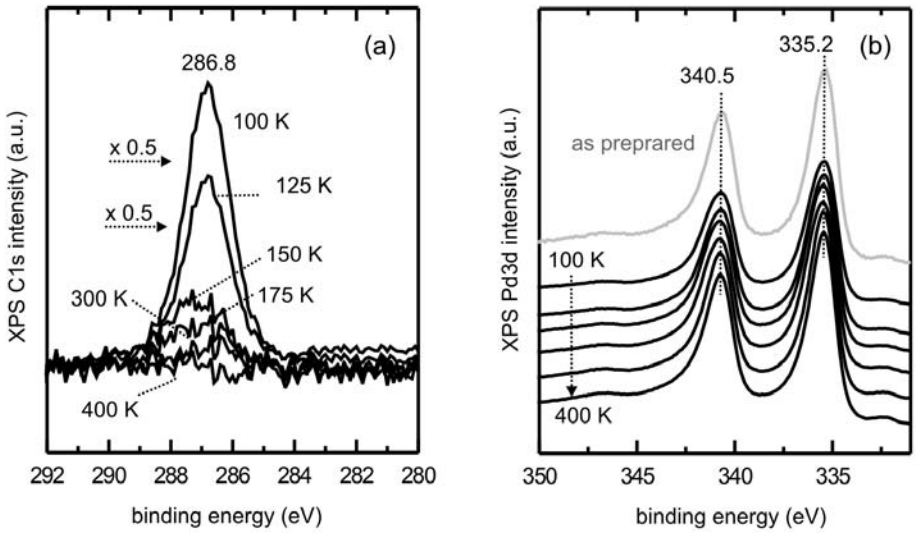


**Figure 4.19:** XPS spectra of methanol TPD on $Pd/Al_2O_3/NiAl(110)$. (a) XPS C1s core-level spectra and (b) corresponding Pd3d lines measured during $CH_3OH$ desorption between 100 and 400 K (exposure: 10 L $CH_3OH$ at 100 K). The Pd3d trace of the Pd particles after preparation is also reported as reference.

Figure 4.19 shows XPS spectra acquired during $CH_3OH$ desorption (initial methanol exposure: 10 L at 100 K) between 100 and 500 K (spectra shown only up to 400 K) on Pd nanoparticles. The interpretation of the spectra is based on the XPS work on Pd(111) presented in this thesis and on previous TPD experiments on the same model catalyst [37, 145]. The XPS spectra in the C1s region are reported in Fig. 4.19a. At 100 K, $CH_3OH$ multilayer is present, producing a single C1s peak with a binding energy (BE) of 286.8 eV (as observed for methanol adsorption on Pd(111)). The thick methanol overlayer reduces the Pd3d signal, as can be observed comparing the Pd3d signal at 100 K with the signal for the clean system (upper grey trace in Fig. 4.19b). The intensity decrease of the C1s signal observed at 125 K may be due to partial desorption of the multilayer, which leads to a slight increase in the corresponding Pd3d signal. Upon increasing the temperature to 150 K a strong reduction of the C1s intensity is observed due to the $CH_3OH$ multilayer desorption. Based on earlier vibrational studies [37,144], the broad C1s signal around 287-286.7 eV observed at 175 K, may be attributed to molecular methanol and methoxy species formed by partial $CH_3OH$ dehydrogenation. At 300 K the dehydrogenation process is probably complete and the small C1s signal at ~286.5 eV is only due to CO, as confirmed by IRAS studies [145]. No carbonaceous species can be observed at BE ~284 eV, indicating that $CH_3OH$ desorption dominates under the applied conditions. At 400 K CO almost completely desorbs and the corresponding Pd3d signal is completely restored. The Pd3d binding energy does not shift during $CH_3OH$ adsorption/desorption experiment with respect to the BE of the pristine sample[7].

As already observed for Pd(111) single crystal ([130] and Fig. 4.1), also for the $Pd/Al_2O_3/NiAl(110)$-system methanol desorption dominates under the applied conditions: modest CO formation is observed and C-O bond scission is negligible under UHV conditions.

[7] The size-dependent shifts of core level BE for metal particles is a well know effect; an increase in BE is observed upon decreasing the particle size. This phenomenon explains the observed higher Pd3d BE in Fig. 4.19b ($Pd3d_{5/2}$ = 335.2 eV) for the alumina supported particles with respect to the Pd bulk metal ($Pd3d_{5/2}$ = 334.9 eV).

### 4.2.2 Methanol decomposition at $10^{-6}$ mbar on $Pd/Al_2O_3/NiAl(110)$

As for Pd(111) single crystal, the $CH_3OH$ pressure on Pd particles was increased in order to enhance the probability of methanolic C-O bond breaking. Figure 4.20a shows a PM-IRAS spectrum of ~$10^{-5}$ mbar methanol after 90 minutes exposure on Pd particles at 300 K. The broad and small signals around 1920 and 1840 $cm^{-1}$ are due to the decomposition product CO. No significant changes were observed in the CO stretching mode during methanol exposure. No other intermediate species can be detected on the surface.

Figure 4.20b shows the corresponding C1s XPS spectra with increasing exposure time. (The corresponding Pd3d signals decrease slightly and shift to higher BE of only +0.1 eV; spectra not shown). Fig. 4.20c displays the quantitative analysis (using the 0.5 ML CO saturation coverage on Pd particles at 300 K as reference). Apparently, a CO coverage of ~0.45 ML is instantaneously produced while the amount of $CH_x$ (formed by C-O bond scission) grows with time until ~0.9 ML $CH_x$ have been formed after ~400 min. The CO coverage seems basically unaffected which agrees with the absence of spectral changes in PM-IRAS. A similar observation has been reported for Pd(111) and attributed to carbon formation and (partial) carbon dissolution in the Pd bulk (which explains why the CO layer is hardly affected).

The dashed line in Fig. 4.20c shows the result of methanol decomposition under similar conditions on Pd(111) (C1s XPS intensities have been normalized by the Pd3d signals both for Pd(111) and Pd nanoparticles). For both surfaces the kinetics of $CH_x$ formation is similar up to 100 min, but upon prolonged methanol exposure a higher $CH_x$ concentration is reached on Pd particles. This may be due to a loss of $CH_x$ via dissolution in the Pd single crystal bulk. In contrast, the small size of Pd particles allows to detect basically all (surface and dissolved) carbon by XPS. It is also reasonable to assume that the higher fraction of low-coordinated sites on Pd particles (such as edges which may be more efficient for C-O bond scission) finally leads to higher $CH_x$ amounts. A maximum coverage of 0.9 ML $CH_x$ is observed after ~400 min $5x10^{-7}$ mbar $CH_3OH$ exposure, suggesting that a high fraction of the particle surface is covered by $CH_x$ under these conditions.

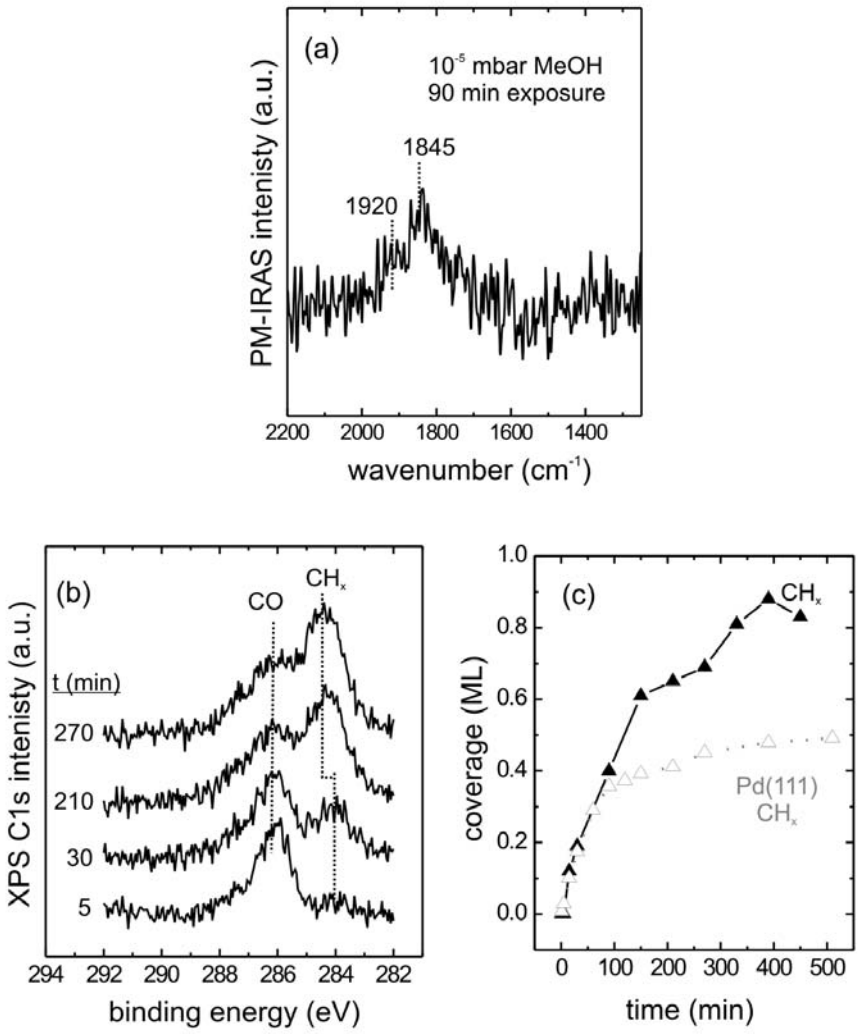


**Figure 4.20:** Methanol on $Pd/Al_2O_3/NiAl(110)$ at 300 K: (a) $10^{-6}$ mbar $CH_3OH$ after 90 min of exposure detected by PM-IRAS; (b) XPS C1s core-level spectra measured during exposure of Pd particles to $5x10^{-7}$ mbar methanol at 300 K. The quantitative analysis of the XPS spectra is shown in (c), and compared to results on Pd(111).

A similar kinetic effect during methanol decomposition on Pd nanoparticles was already observed [78,105]. From the analysis of TR-IRAS (time-resolved reflection-absorption IR spectroscopy) data, it was found that the rate of carbon formation was high on the pristine Pd particles, while the rate decreased rapidly with increasing carbon coverage. This behavior was attributed to a fast C-O bond breakage only at the defects sites (i.e. particle edges and steps), which are poisoned during the reaction, but not at the regular facets. The

authors concluded that the activity for C-O bond scission was drastically enhanced at the particle defect sites and that the carbon species formed by methanol decomposition preferentially accumulated at defect sites. Unfortunately a precise ratio of the $CH_x$ formation on the different sites (defect sites *vs.* sites on regular (111) terraces) was not specified. In a following publication, *Schauermann* [note 7, page. 79 in 144] did not exclude the possibility that the C-O bond scission could take place also on the regular (111) facets, but at a much lower rate.

### 4.2.3 Methanol oxidation on $Pd/Al_2O_3/NiAl(110)$

Partial oxidation of methanol on Pd-$Al_2O_3$ was carried out with 15 mbar $CH_3OH$, 15 mbar $O_2$ and 1050 mbar He as fill-up gas to atmospheric pressure, at temperatures ranging from 300 to 475 K (Figure 4.21a). As reported in the literature [37,144,145], methanol adsorbs on alumina, but blank experiments did not report any activity of the $Al_2O_3$ support for methanol oxidation. On Pd-$Al_2O_3$ at 300 and 350 K no methanol conversion can be detected by GC. The onset of catalytic activity is observed at 400 K; at this temperature a $CH_3OH$ conversion of ~90% is reached after several hours. In Fig. 4.21b selectivity *vs*. time is plotted for methanol oxidation on Pd particles at 400 K (15 mbar $CH_3OH$, 15 mbar $O_2$ and 1050 mbar He as fill-up gas to atmospheric pressure). Apparently, the selectivity is quite constant with reaction time. As for Pd(111), water, $CO_2$ and formaldehyde were observed as products during methanol oxidation on Pd particles. Ethanol was also observed (ca. 23 %), suggesting the involvement of $CH_3$ groups in the reaction (an explanation about ethanol formation was already suggested in section 4.1.3 for methanol oxidation on Pd(111) under similar conditions).

Figure 4.21c shows PM-IRAS spectra of methanol oxidation on Pd particles at 300-400 K. On the pristine sample 5 mbar $CH_3OH$ were dosed at 300 K (trace 1) and only a weak broad signal can be observed, due to the dehydrogenation product CO (1830-1730 $cm^{-1}$; CO on hollow sites). When 5 mbar $O_2$ where added at 300 K, no spectral changes could be observed (spectrum not shown). Traces 2 and 3 correspond to methanol oxidation at 400 K after 10 and 30 min of reaction, respectively. The CO peak shifts to 1920 $cm^{-1}$ (hollow/bridge bonded CO) and increases slightly in intensity. The surface of Pd particles is probably more free from the carbonaceous deposit (formed by the methanolic C-O bond

scission at 300 K), presumably via $CH_x$ oxidation to CO or $CO_2$ at higher temperature. Unfortunately, due to the low quality of the PM-IRAS spectra a detailed analysis of the gas phase spectra could not be performed[8]. Nevertheless, it can be concluded that the catalytic activity is very similar for Pd particles and Pd(111).

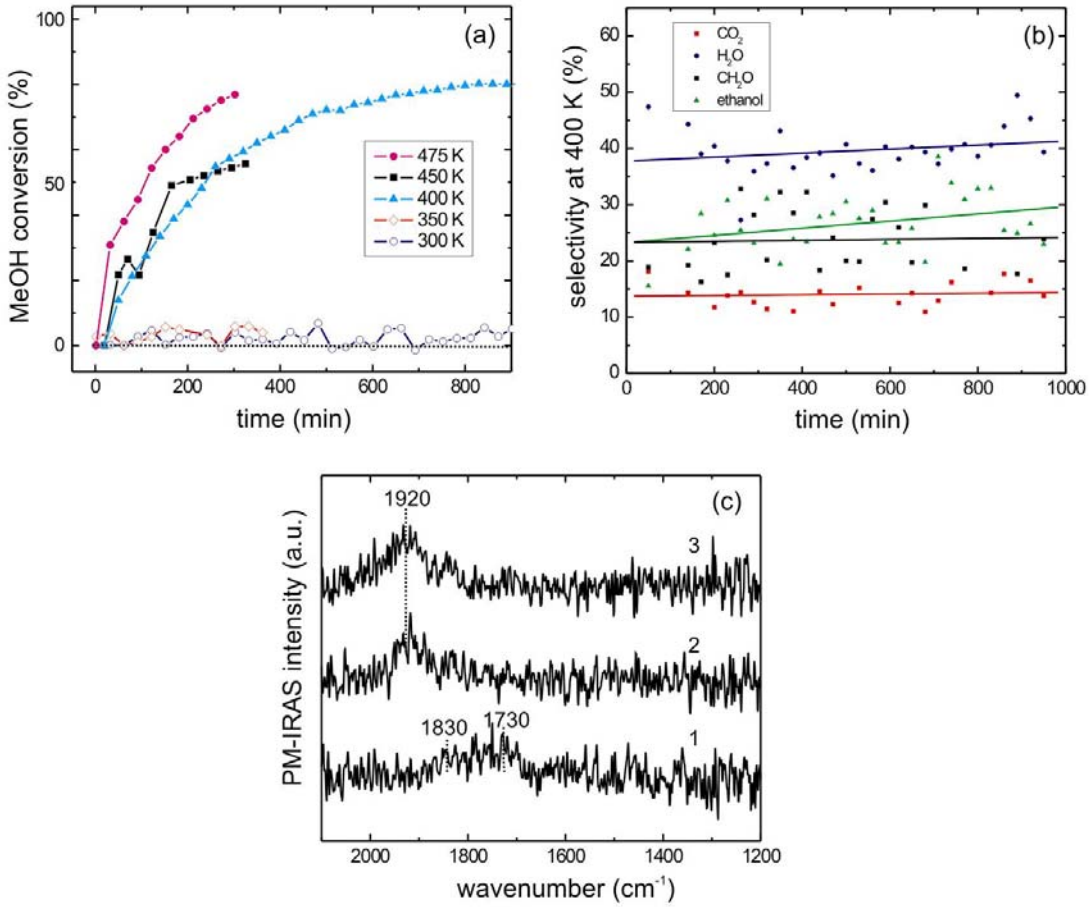


**Figure 4.21:** Gas chromatography analysis (a, b) measured during $CH_3OH$ oxidation on Pd-$Al_2O_3$ at 300-475 K (15 mbar $CH_3OH$, 15 mbar $O_2$, 1050 mbar He as carrier gas). (c) PM-IRAS spectra measured during $CH_3OH$ oxidation at 300-400 K (5 mbar $CH_3OH$ added at 300 K prior to 5 mbar $O_2$ (trace 1)). Spectra 2 and 3 were acquired during the oxidation reaction at 400 K, after 10 and 30 min, respectively.

Complementary information can be obtained from *in-situ* SFG experiments performed recently in our group [37]. 15 mbar $CH_3OH$ plus 15 mbar $O_2$ were dosed at 300-450 K on alumina supported Pd particles. At 300 K a reduced CO coverage (~0.3 ML) was observed,

[8] The low intensity of the PM-IRAS was due to a malfunction of the resonant circuit, which compromised the experiments in the last months of work during this thesis. The same experiment was repeated again, but it was not possible to obtain better results.

due to the hindering effect of oxygen towards methanol dehydrogenation (which is a previous step of the oxidation process). Also the formation of $CH_x$ species at 300 K contributes to the low CO coverage. As confirmed by GC analysis, no catalytic activity was observed due to surface poisoning by CO, $CH_x$ and oxygen, and a minimum temperature of 400 K was again needed to obtain conversion.

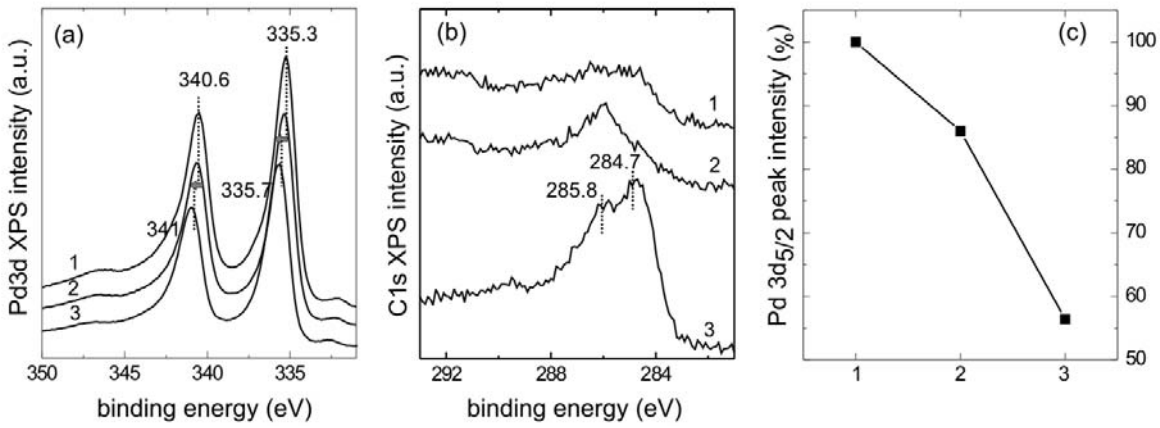


**Figure 4.22:** Pre- and post-reaction XPS spectra in the Pd3d (a) and C1s (b) region, measured on Pd-$Al_2O_3$: as prepared (spectrum 1); after sample stabilization (spectrum 2); after mbar reaction at 400 K (spectrum 3). (c) shows the change in intensity of the $Pd3d_{5/2}$ signal for Pd-$Al_2O_3$ as prepared (1), after stabilization (2) and after mbar reaction at 400 K (3).

It is now interesting to consider the pre- and post-reaction XPS spectra (to quench the reaction the gas was quickly evacuated and the temperature rapidly lowered). The Pd3d and C1s regions are displayed in Figure 4.22. No clear information could be extrapolated from the analysis of the O1s region, because of the overlap of $Pd3p_{3/2}$ and O1s signals and due to emissions from O1s core levels of the alumina support (peak at 531.5 eV).

After the "stabilization procedure" (for details the reader is referred to section 2.6.2), no shift in the Pd3d BE and a small increase in the amount of adsorbed CO are observed (Fig. 4.22a and b trace 2 of, respectively). The intensity of the $Pd3d_{5/2}$ peak decreases ~10% after the stabilization (Fig. 4.22c). A former combined STM, AES, LEED, PES, TPD and molecular beam study on the same model catalyst [52] has shown that the morphology and the distribution of particles on the surface remain essentially unchanged after oxygen exposure at 480 K. However, an increase in the thickness of the alumina support was observed. A sintering of the Pd particles during stabilization can be excluded. The

decreased intensity in the Pd3d signal can be due to the residual amount of CO on the surface (Fig. 4.22b, trace 2).

Two pronounced differences can be observed after the catalytic reaction at ambient pressure and 400 K (~60 min):

(i) About 0.8 ML $CH_x$ were detected, i.e. substantial amounts of carbonaceous species were present during the reaction. These $CH_x$ species (which are, as mentioned, most likely elemental carbon), can not only be located on the Pd particle surface (since previous SFG studies [37] and the current PM-IRAS spectra indicated CO coverages around 0.5 ML), but must in part reside in subsurface regions. The $CH_x$ species may not only be undesired poisons but may favorably affect the reaction. Time-resolved PM-IRAS performed on Pd(111) has suggested that carbonaceous overlayers may in fact stabilize surface $CH_2O$ species, and thus favor the partial oxidation product $CH_2O$ (section 4.1.2 and 4.1.3).

(ii) Fig. 4.22a shows the Pd3d spectra before and after the high pressure reaction. Although the PM-IRAS peak positions of CO observed during the reaction are characteristic of adsorption on *metallic* Pd, the ~+0.4 eV binding energy shift suggests that the Pd particles became partially oxidized during the methanol oxidation reaction (by contrast, full oxidation to PdO particles would result in binding energy shifts of ~+1.5 eV). This finding is remarkable in the sense that identical XPS measurements on Pd(111) indicated that the Pd(111) single crystal surface *remained metallic* during methanol oxidation. Apparently, Pd nanoparticles are easier to oxidize, presumably due to the higher abundance of surface defects. Oxide formation at the Pd-alumina interface may also contribute to the Pd3d spectra [146].

The oxidation behavior of Pd model catalysts under UHV will be presented in the following section.

## 4.3 Pd oxidation in UHV

The formation of oxides on metal surfaces has raised much attention because of the fundamental importance of oxidation processes. Recently the interest has been focused on understanding the role that oxides can play during a catalytic reaction [140].

Palladium is used in many oxidation reactions and it has been suggested that its oxidized phase plays an active role for the removal of hydrocarbons and CO in car exhaust converters and in the combustion of methane [147,148]. Several studies [142,149-151] have investigated the interaction of palladium with oxygen under low pressure conditions ($<10^{-6}$ mbar). On the Pd(111) surface, adsorption of oxygen at 300 K results in a (2x2)-$O_{ads}$ structure corresponding to a coverage of 0.25 ML [142,151,152]. As reported by *Lundgren et al.* [143], after exposure of Pd(111) to oxygen at 600 K an incommensurate two-dimensional (2D) surface oxide is formed, $Pd_5O_4$. There are two kinds of oxygen atoms in the $Pd_5O_4$ layer. Half of the oxygen atoms are three-fold coordinated and bonded only to in-plane Pd atoms, the other half is four-fold coordinated and bonded also to the sub-surface Pd atoms, above which they are located. Four palladium atoms per unit cell are coordinated to two neighbouring oxygen atoms. The remaining Pd atom is coordinated to four oxygen atoms. This structure has neither the stoichiometry nor structure similarity to any plane of the bulk PdO oxide [153]. DFT calculations [143,154,155] have determined the Pd-O phase diagram revealing that the two-dimensional $Pd_5O_4$ is thermodynamically stable at intermediate oxygen pressures, between the stability ranges of the (2x2)-$O_{ads}$ adlayer and of the bulk oxide PdO. TPD experiments [156] confirmed the oxygen coverage calculated in [143] for $Pd_5O_4$ to be $1/\sqrt{3} = 0.58$ monolayers oxygen, with reference to bulk terminated Pd(111). Recently [157] the interaction of palladium with oxygen was investigated by *in-situ* XPS at elevated pressure. The Pd(111) surface was completely covered with the $Pd_5O_4$ oxide by heating in $3x10^{-3}$ mbar $O_2$ between 598 K and 654 K. The 2D oxide was characterized by two O1s components at 528.92 eV and 529.52 eV and by two oxygen-induced $Pd3d_{5/2}$ components at 335.5 eV and 336.24 eV. By changing the photon energy, the authors could confirm the surface nature of this 2D oxide. Increasing the temperature, the 2D oxide starts to decompose and above 717 K diffusion of oxygen in the palladium bulk occurs. The structure of $Pd_5O_4$ has been resolved, but its catalytic behaviour is still unknown.

In order to investigate the effect of surface structure on the oxidation of palladium, the same oxidation conditions ($10^{-5}$ mbar $O_2$ at 650 K for 15 min) were applied to Pd(111) single crystal, to a thin (111) oriented Pd film on NiAl(110) and to Pd nanoparticles supported on $Al_2O_3$/NiAl(110). The reactivity of the oxides formed on the different Pd model catalysts towards CO was also studied.

### 4.3.1 Oxidation of Pd(111)

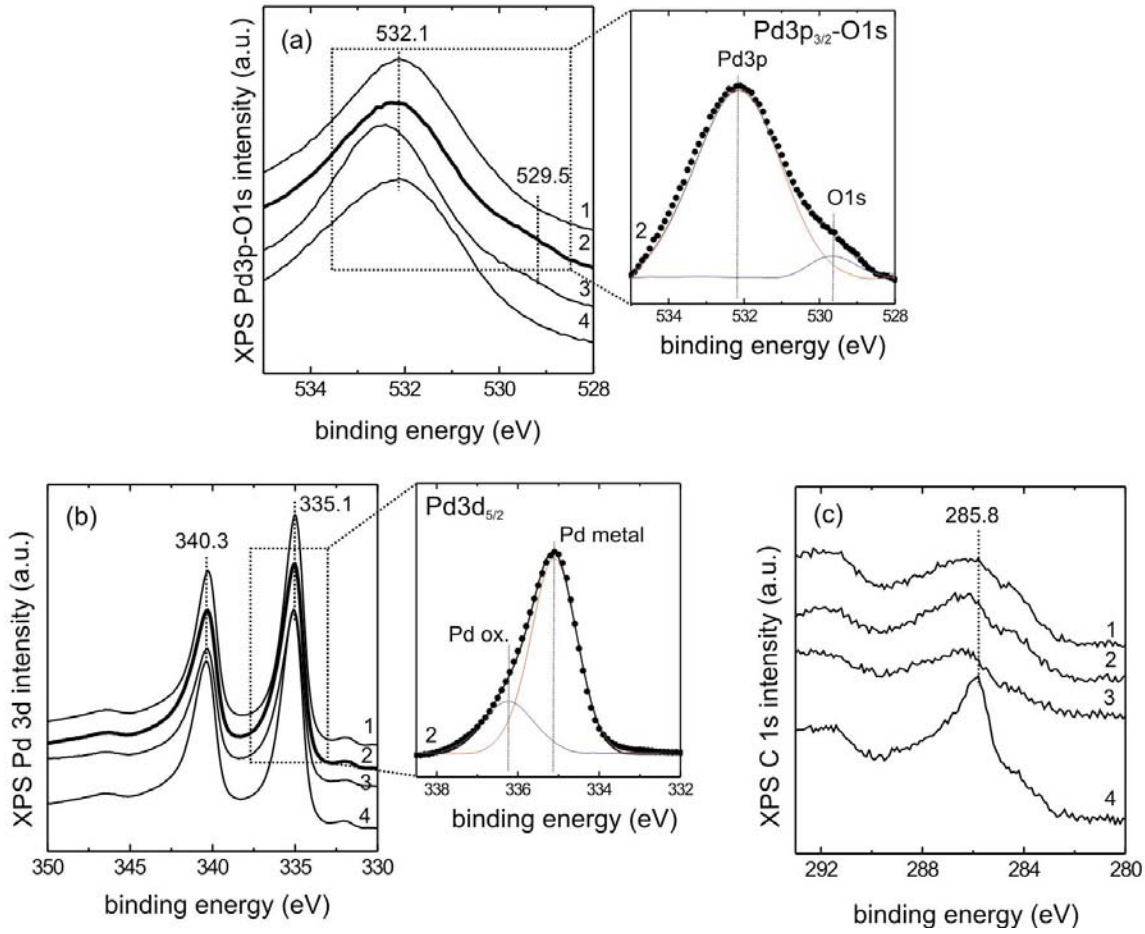


**Figure 4.23:** Oxidation of Pd(111). XPS spectra in the O1s (a), Pd3d (b) and C1s (c) region: as prepared (spectrum 1); after oxidation at $10^{-5}$ mbar $O_2$ at 650 K (spectrum 2); after reaction with $10^{-7}$ mbar CO at 100 K (spectrum 3) and at 300 K (spectrum 4). The fitting curves for the $Pd3d_{5/2}$ and Pd3p-O1s regions after the oxidation (traces 2) are also reported. Pd-satellite peaks due to the non-monochromatic X-ray source used (see section 2.2) are visible in the spectra in the C1s region (c).

Figure 4.23 shows O1s, Pd3d and C1s XPS spectra for Pd(111) for various conditions. Upon oxidation in $10^{-5}$ mbar $O_2$ at 650 K (15 min) a weak O1s signal is observed at 529.5 eV and shoulders appeared at the high binding energy side of the Pd3d peaks (336.2 and 341.6 eV) (traces 2 in Fig. 4.23a and b, respectively). These values are typical for the formation of a $Pd_5O_4$ surface oxide, which exhibits a two-dimensional structure having no resemblance to any bulk oxides of Pd [143,157,158]. No shift of the bulk component in the

Pd3d XPS peaks is observed. At 100 K CO does not adsorb on $Pd_5O_4$ (Fig. 4.23, traces 3), suggesting that most of the single crystal surface is oxidized. At higher temperature, however, the surface oxide is quite reactive, as shown by its removal by CO exposure at 300 K (disappearance of the shoulders in the Pd3d and O1s regions, and CO adsorption on the Pd surface; Fig. 4.23, traces 4).

Similar results as for Pd(111) were obtained for a (111) oriented thin Pd film deposited on NiAl(110) (thickness ~30 nm) under the same oxidation conditions (spectra not shown).

Earlier studies reported Pd3d peak shifts between 1.1 and 1.9 eV for strongly oxidized Pd or PdO powders [158 and references therein]. During high pressure oxidation (1 Torr), *Kettler et al.* [158] recently observed the formation of PdO on Pd(111), characterized by a single peak shifted by ~1.6 eV compared to bulk metallic Pd. For smaller binding energy shifts, the authors suggested the presence of "subsurface oxide" which can be observed over an extended pressure and temperature range.

### 4.3.2 Oxidation of $Pd/Al_2O_3/NiAl(110)$

Figure 4.24 collects the results for oxidation treatments on alumina supported Pd nanoparticles. The stabilization procedure to increase the thermal stability of the Pd particles does not induce BE shifts (as already discussed) (traces 2 and 3). Annealing to 650 K in vacuum did also not change the Pd3d binding energy (trace 4). Oxidation of Pd nanoparticles in $10^{-5}$ mbar $O_2$ at 650 K (15 min) induced a Pd3d BE shift of +0.6-0.7 eV (trace 5), similar to that after the high pressure oxidation reaction (Fig. 4.22). This proves an oxidation of the Pd particles because thermal annealing at 650 K alone (in the absence of oxygen) had no effect. Therefore, Pd particle sintering (which may also lead to a BE shift) can be excluded. A reduction in CO at 650 K (trace 6) only partly reversed the Pd3d BE shift observed after Pd nanoparticles oxidation. In a recent work [146], the oxidation behaviour of three-dimensional Pd clusters supported on $Fe_3O_4$ was investigated by high-resolution XPS using synchrotron radiation. For the clean Pd particles the $Pd3d_{5/2}$ peak was fitted to two features at 335.0-335.1 eV (Pd bulk signal) and at 335.3-335.6 eV (surface- and interface-derived component). After oxygen exposure at 600 K (pulse of $O_2$ for 100 s), components at higher BE were observed. Based on previous work on single crystal surfaces

[143,159], the authors decomposed the $Pd3d_{5/2}$ component in three regions related to: 1) Pd bulk metal (335.0-335.1 eV); 2) metallic Pd coordinated to chemisorbed oxygen and from specific Pd atoms in thin oxide layers (~335.7 eV); 3) Pd atoms in thin oxide layers only (~336.6-336.7 eV). The shift to 335.6 eV (and the asymmetry towards higher BE) observed in the present work for the oxidized $Pd/Al_2O_3/NiAl(110)$ system is consistent with the finding for $Pd/Fe_3O_4/Pt(111)$ [146]. Anyway, high resolution XPS using synchrotron radiation is required for more precise assignments.

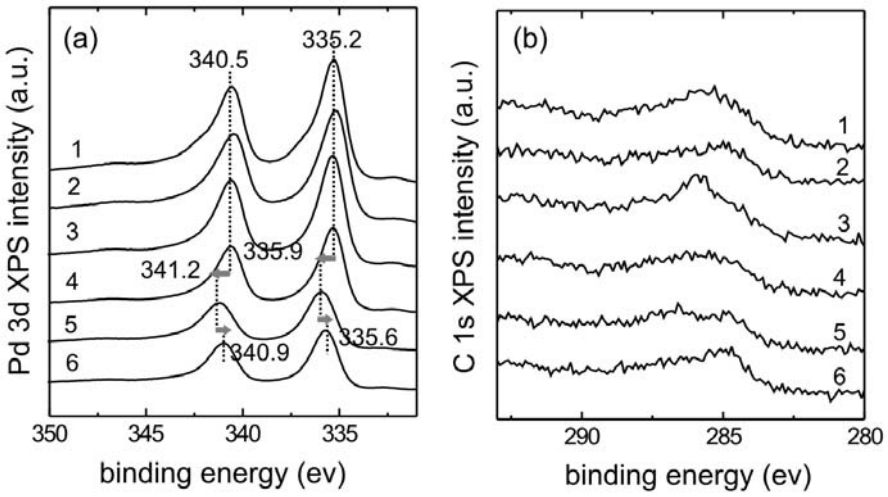


**Figure 4.24:** Oxidation of $Pd/Al_2O_3/NiAl(110)$. XPS spectra in the Pd3d (a) and C1s (b) regions: as prepared (spectrum 1); during stabilization procedure in $10^{-6}$ mbar $O_2$ at 490 K (spectrum 2); after sample stabilization (spectrum 3); after annealing at 650 K in UHV (spectrum 4); after oxidation at $10^{-5}$ mbar $O_2$ at 650 K (spectrum 5); after reaction with $10^{-6}$ mbar CO at 650 K and cooling in UHV to 300 K (spectrum 6). All the spectra were acquired at 300 K.

In order to quantify the degree of Pd particle surface oxidation, i.e. whether the Pd surface was fully oxidized or whether there was a coexistence of metallic and oxidic areas, CO adsorption was performed on a freshly oxidized sample ($10^{-5}$ mbar $O_2$ at 650 K (15 min)). $10^{-7}$ mbar CO were dosed for 5 minutes (30 L CO) at 450 K on the oxidized Pd particles in order to react residual physisorbed oxygen away (leaving at least the non-reactive oxide unaffected). No changes in the Pd3d region were observed (spectrum not shown). The system was then cooled in the presence of CO ($10^{-7}$ mbar) to 300 K. The corresponding Pd3d XPS spectrum (Fig. 4.25a, trace 3) shows that the BE shift due to the oxidation treatment is not reversed, while in the C1s region only a CO coverage of ~0.23

ML is observed (Fig. 4.25b, trace 3) (CO saturation on Pd particles at 300 K corresponds to 0.5 ML, as shown by trace 2). For Pd nanoparticles about 50% of the Pd particle surface is no longer accessible to CO and thus oxidized, indicating a *partial surface oxidation* of the Pd nanoparticles (similar to the situation after the high pressure reaction of Fig. 4.21). The treatment in CO at 300 K is not sufficient to reduce the (partial) oxidation of the surface.

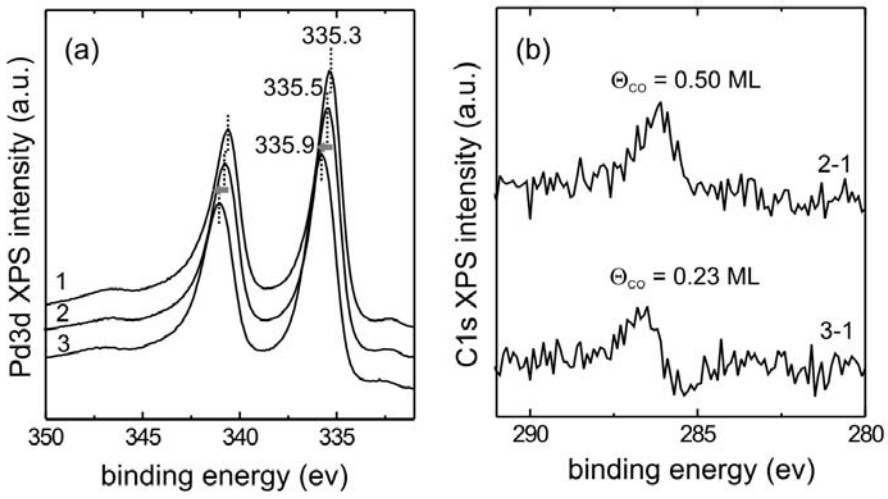


**Figure 4.25:** CO adsorption on oxidized Pd particles in the Pd3d region (a): as prepared (spectrum 1); reference CO saturation coverage at 300 K (spectrum 2); in $10^{-7}$ mbar CO at 300 K after oxidation at 650 K (spectrum 3). In the C1s region (b) the difference spectra (2-1) and (3-1) are reported.

The surface oxide on three-dimensional Pd particles can be reacted (reduced) with CO, similar as for Pd(111). However, oxidation behaviour for Pd particles differs from the behaviour observed for the Pd(111) single crystal. In fact, for Pd(111) the high BE side shoulders disappeared already for CO treatment at 300 K, while for Pd nanoparticles the Pd3d BE shift can only be *partly reversed* by reaction with CO at 650 K. This indicates that not all of the Pd-oxide is located at the surface but also extends into the particle and may even be located at the metal-oxide interface, as reported for the Pd-$Fe_3O_4$ system [146]. The partial reversal of the BE shift is another argument against particle sintering because it is very unlikely that sintering is easily reversed by CO treatment. The exact nature of the oxide phase on Pd nanoparticles has not been fully identified yet, though. Nevertheless, the observed binding energies are comparable to a $Pd_5O_4$ surface oxide which may grow on the (111) particle facets while stoichiometric PdO can be excluded (the BE shift would then be

~+1.5 eV). It is also plausible anyway that oxides of different nature have been formed on Pd(111) and on Pd particles, explaining the different reactivity towards CO.

## 4.4 Summary

Methanol adsorption and reaction on Pd(111) and $Pd/Al_2O_3/NiAl(110)$ were investigated under UHV and higher pressure in a wide temperature range between 100 K and 550 K.

A combined PM-IRAS and XPS study of methanol adsorption/desorption reported similar behavior for smooth Pd(111), ion-bombarded Pd(111) and alumina supported Pd nanoparticles under the same conditions. Under UHV, methanol desorption dominated and C-O bond scission was negligible for all the Pd systems. At higher pressure ($\sim 10^{-6}$ mbar) and higher temperature (300-450 K) significant amounts of carbon deposits were detected by XPS, suggesting a considerable activity of Pd model catalysts for methanolic C-O bond breaking under the given conditions. *In-situ* PM-IRAS spectra detected CO, formaldehyde ($CH_2O$) and formyl (CHO) during methanol decomposition on Pd(111) at 300 K. It was shown that carbonaceous species have an influence on the different $CH_xO$ species formed during methanol dehydrogenation on Pd(111).

The nature, structure and morphology of the methanol-derived carbon deposit were investigated by a combination of angular-resolved XPS, STM and LEED. Monolayer thick (~2.3 Å) carbon islands grew randomly all over the Pd(111) surface and presented a hexagonal arrangement with unit cell of ~7 Å. The carbon overlayers also caused a rearrangement of the Pd atoms, as the Pd step edges appeared rough and irregular after long methanol exposure.

Methanol oxidation at millibar pressure between 300 and 475 K was followed by PM-IRAS and GC on Pd(111) single crystal and on Pd nanoparticles. On both systems, CO was spectroscopically observed on the surface during reaction at 400 K. Formaldehyde and formyl have been detected together with CO on the Pd(111) single crystal surface during millibar exposure at 300 K. The main oxidation products observed by GC for both Pd model catalysts were $CO_2$, $H_2O$ and $CH_2O$. The gas phase composition during a reaction was followed by *in-situ* PM-IRAS (p+s) gas phase spectra, in agreement with the data obtained using gas chromatography.

Post-reaction XPS after methanol oxidation at ambient pressure and 400 K detected carbon deposit on both Pd systems. Carbonaceous species during methanol oxidation may favourably affect the reaction influencing the selectivity. An interesting difference was observed between Pd(111) and $Pd/Al_2O_3/NiAl(110)$: while no BE shift was observed in the Pd3d region for the Pd(111) single crystal, a shift of ~+ 0.4 eV was reported for Pd supported nanoparticles. Under the reported reaction conditions, XPS measurements suggested that Pd(111) remained *metallic*, while Pd nanoparticles became *partially oxidized*.

The nature of the oxides formed during oxygen exposure ($10^{-5}$ mbar) at high temperature (650 K) on Pd(111) and Pd nanoparticles was investigated by XPS. The observed binding energies for both systems were comparable to a two-dimensional $Pd_5O_4$ surface oxide, while the formation of stoichiometric PdO could be excluded. The oxide formed on Pd(111) was completely reacted away by CO exposure at 300 K, while for Pd nanoparticles the Pd3d BE shift could only be *partly reversed* by reaction with CO at 650 K.